APPLIED SCIENCES AND ENGINEERING

Injectable photocurable Janus hydrogel delivering hiPSC cardiomyocyte-derived exosome for post–heart surgery adhesion reduction

Ling Wang[1,2]†, Peier Chen[3,4]†, Yuxuan Pan[3]†, Zihan Wang[2,5], Jie Xu[1], Xiaoqi Wu[6], Qiao Yang[1], Meng Long[2], Sitian Liu[2], Wenhua Huang[2]*, Caiwen Ou[3]*, Yaobin Wu[2]*

Postsurgical pericardial adhesions pose increased risks of sequelae, prolonged reoperation time, and reduced visibility in the surgical field. Here, we introduce an injectable Janus hydrogel, which exhibits asymmetric adhesiveness properties after photocrosslinking, sustained delivering induced pluripotent stem cell–derived cardiomyocyte exosomes (iCM-EXOs) for post–heart surgery adhesion reduction. Our findings reveal that iCM-EXOs effectively attenuate oxidative stress in hydrogen peroxide–treated primary cardiomyocytes by inhibiting the activation of the transcription factor nuclear factor erythroid 2–related factor 2. Notably, in rat cardiac postsurgery models, the Janus hydrogels loaded with iCM-EXOs demonstrate dual functionality, acting as antioxidants and antipericardial adhesion agents. These hydrogels effectively protect iCM-EXOs from GATA^{6+} cavity macrophage clearance by inhibiting the recruitment of macrophages from the thoracic cavity. These results highlight the promising potential of iCM-EXO–laden Janus hydrogels for clinical safety and efficacy validation in trials involving heart surgery patients, with the ultimate goal of routine administration during open-heart surgeries.

INTRODUCTION

During heart surgery, surgical trauma to the epicardium can result in postoperative pericardial adhesions, which are fibrous connections between the epicardium and the chest cavity. These adhesions substantially prolong the cardiopulmonary bypass time and the total operation time, as well as increase the mortality rate of redo cardiac surgery by threefold compared to primary cardiac surgery (*1*, *2*). For children patients with congenital heart disease, approximately 33% of all pediatric and congenital heart surgeries require redo cardiac surgery (*3*). Similarly, at least 12% of adults undergoing valve replacements, mechanical circulatory support, or cardiopulmonary bypass grafting also require redo cardiac surgery (*1*). However, the molecular mechanisms underlying postoperative pericardial adhesions have not been fully elucidated. Nevertheless, previous clinical studies have shown that heart surgeries often result in bleeding (*4*) and pericardial fluid exudation (*5*), which enhance oxidative stress (*6*), and induce the inflammatory response within the pericardial space. These factors are proposed to create a predisposition for the adhesion phenotype (as illustrated in Fig. 1A). Bleeding and pericardial fluid exudation contribute to pericardial adhesion by depositing fibrinogen and collagen and recruiting macrophages from the thoracic cavity (*4*). Excess reactive oxygen species (ROS) can damage mitochondrial membranes, irreversibly injure cells, trigger apoptosis, and contribute to the development and progression of maladaptive myocardial remodeling and heart failure (*6*, *7*). Therefore, effective methods for preventing postoperative pericardial adhesion need to be designed and validated to improve the outcomes of patients undergoing heart surgeries.

Now, available prophylactic options against postoperative pericardial adhesions include commercial solid barriers such as polylactic acid (CardioWrap), liquid solutions such as 0.1% (w/v) sodium hyaluronate, and gel barriers such as polyethylene glycol (Coseal). However, these products do not fully prevent postoperative adhesions as they are only weakly adhesive and cannot completely cover wet tissues in vivo. Moreover, certain solid barriers must be sutured to the target tissues. This treatment may further damage the heart tissue. In addition, as certain gel barriers are highly soluble in the body, they may be cleared from the target sites too rapidly (*8*). In contrast, recent studies have explored adhesive hydrogels resembling those secreted by mussels as postoperative pericardial adhesion barriers (*9*, *10*). They can strongly adhere even to wet tissue surfaces. Unfortunately, while one of their surfaces may adhere to the target tissue, the other could simultaneously adhere to nontarget tissues as well. Therefore, a hydrogel that can robustly adhere to the target tissues and not adhere to the nontarget tissues is of great clinical significance. These Janus hydrogels have drawn a great deal of research attention as they have asymmetric adhesiveness. They demonstrated antiadhesive efficacy in the abdominal wall and gastric perforations (*11*–*13*). We recently reported an injectable photocurable Janus hydrogel based on grafting catechol groups, which was named HAD [hyaluronic acid–*g*-(2-aminoethyl methacrylate hydrochloride–dopamine)]. It effectively prevented postoperative abdominal adhesion (*12*). One side of HAD hydrogel adheres to wet tissues, while the other resists tissue adhesion. In this manner, the HAD hydrogel acts as a physical barrier between

[1]Biomaterials Research Center, School of Biomedical Engineering, Southern Medical University, Guangzhou 510515, China. [2]Guangdong Engineering Research Center for Translation of Medical 3D Printing Application, Guangdong Provincial Key Laboratory of Digital Medicine and Biomechanics, Department of Human Anatomy, School of Basic Medical Sciences, Southern Medical University, Guangzhou 510515, China. [3]Affiliated Dongguan Hospital, Southern Medical University (Dongguan People's Hospital), Dongguan 523058, China. [4]Department of Cardiology, Laboratory of Heart Center, Heart Center, Zhujiang Hospital, Southern Medical University, Guangzhou 510280, China. [5]Department of General Surgery, Nanfang Hospital, Southern Medical University, Guangzhou 510515, China. [6]Department of Urology and Andrology, Ren Ji Hospital, School of Medicine, Shanghai Jiao Tong University, Shanghai 200001, China.
*Corresponding author. Email: wuyaobin2018@smu.edu.cn (Y.W.); oucaiwen@smu.edu.cn (C.O.); hwh@smu.edu.cn (W.H.)
†These authors contributed equally to this work.

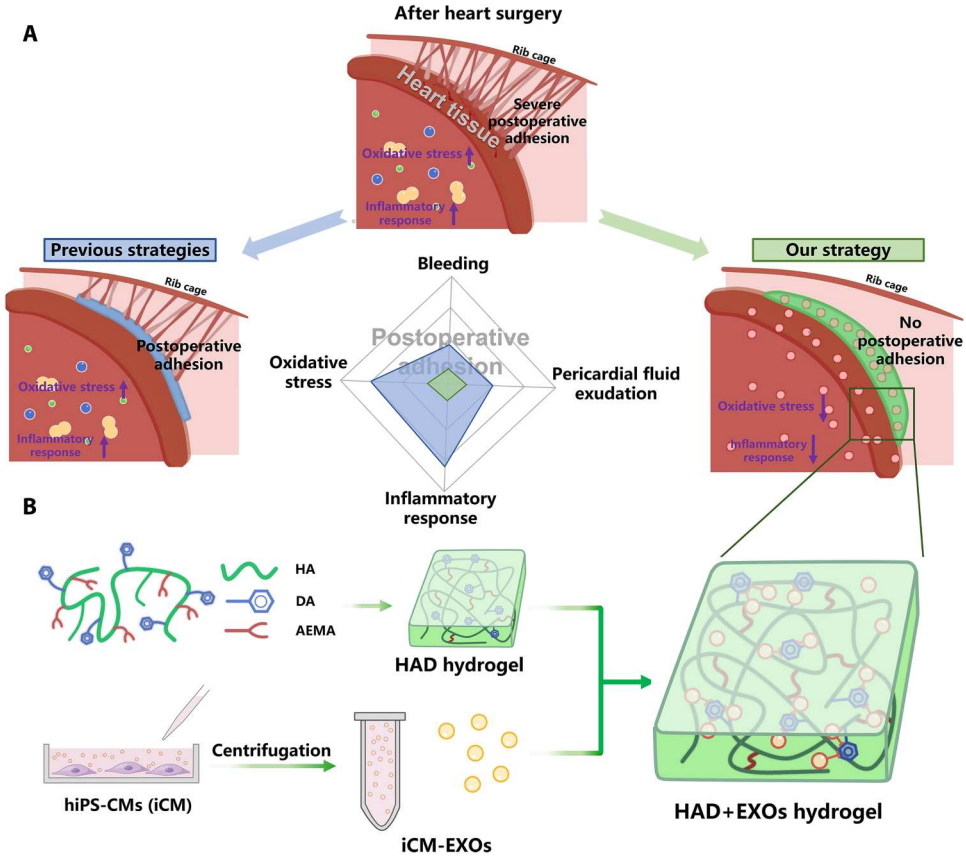

Fig. 1. Overview of HAD+EXOs hydrogel for preventing postoperative adhesion after heart surgery. (**A**) Schematic representation of postoperative pericardial adhesion. Bleeding, pericardial fluid exudation, oxidative stress, and inflammatory response are associated with severe postoperative pericardial adhesion. Previous investigations applied hydrogels or film barriers to staunch bleeding or pericardial fluid exudation. Nevertheless, these modalities failed to reduce oxidative stress and the inflammatory response. (**B**) We exploited the catechol groups in DA to create an injectable, photocurable Janus HAD hydrogel with asymmetric adhesion and ability to provide sustained release of hiPSC cardiomyocyte–derived exosomes that mitigate oxidative stress and inflammatory response. In this manner, the HAD and the exosomes synergistically prevent or mitigate postoperative pericardial adhesion.

adjacent tissues. Unfortunately, few prior investigations have reported the application of hydrogel barriers with asymmetric adhesive properties for the prevention of postoperative pericardial adhesions. The existing adhesive hydrogels were designed to prevent postoperative adhesions by serving as physical barriers. While they could staunch bleeding or pericardial fluid exudation during heart surgery, they could not mitigate the oxidative stress and inflammatory response within the pericardial space. Therefore, it would be highly beneficial for designing hydrogel with dual effects of reducing postoperative adhesion and against oxidative stress for patients suffering from cardiac surgeries.

Exosomes have been shown to potentially affect endogenous repair in the heart by mediating proangiogenic, antiapoptotic, and anti-inflammatory responses (*14*). Exosomes derived from mesenchymal stem cells (*15*), cardiac progenitor cells (*16*), and induced pluripotent stem cells (iPSCs) (*17*) have been shown to reduce oxidative stress and provide protective preconditioning when injected into mouse hearts. Exosomes from undifferentiated iPSCs (iPSC-EXOs) may offer benefits, while their composition will reflect their originating cells′ undifferentiated state. This might make them more general in their effects. In addition, exosomes from iPSC-derived cardiomyocytes (iCM-EXOs) have been found to have cardioprotective efficacy, improving the left ventricular ejection fraction and myocardial viability (*18*). Another pioneering study showed that iPSC-derived cardiomyocytes, unlike naive iPSCs, secrete exosomes carrying cardiomyocytes-specific cargo that can target the myocardium both by protecting from injury and by promoting recovery after injury in infarcted rat hearts (*19*). However, the efficacy of iCM-EXOs in alleviating oxidative stress still needs to be determined. One challenge in using exosomes therapeutically is that intravenously injected exosomes are rapidly cleared by macrophages and tend to accumulate in the liver, spleen, and lungs (*20*, *21*). Therefore, the efficient delivery of exosomes to the heart and the maintenance of their stability and biological potency there remain challenging (*22*). Hydrogels could potentially deliver large numbers of exosomes to the heart through sustained release and provide superior cardiac function improvement compared to exosomes alone (*23*, *24*). Therefore, we hypothesize that an ideal hydrogel could protect exosomes from clearance by macrophages from the thoracic cavity and enhance the effects of exosomes. Moreover, an adhesive hydrogel may facilitate the sustained release of exosomes from hydrogel to the target tissue by increasing the contact surface and reducing the diffusion.

In the present work, we encapsulated iCM-EXOs in HAD hydrogels with asymmetric adhesiveness and obtained HAD+EXOs hydrogels with the ability to mitigate oxidative stress and reduce pericardial adhesion after cardiac surgery (Fig. 1B). The asymmetric adhesive characteristics of HAD hydrogel including its adhesive strength and antiadhesion property were empirically demonstrated in this study. We also investigated the antioxidant efficacy of iCM-EXOs here. The sustained release of iCM-EXOs from HAD+EXOs hydrogel and its effect on oxidative stress damage to the myocardium were investigated both in vitro and in vivo. We also assessed the antiadhesion and antioxidant efficacies of HAD+EXOs hydrogel in a rat postcardiac surgery model and monitored the performance of the hydrogel for 4 weeks after surgery. We hypothesized that the HAD+EXOs hydrogel could effectively inhibit or prevent pericardial adhesion and mitigate oxidative stress after heart surgery.

RESULTS

The HAD precursor was synthesized by grafting dopamine hydrochloride (DA) and 2-aminoethyl methacrylate (AEMA) onto the hyaluronic acid (HA) chain according to our previously reported methodology (*12*). We selected HA as the main chain because this polyanionic ligand is widely used as an antiadhesive barrier in clinical applications (*25*). HA was endowed with adhesive groups (DA) and photocurable groups (AEMA) to functionalize it with adhesiveness and photocrosslinking, respectively (Fig. 2A). Hyaluronic acid–*g*-(2-aminoethyl methacrylate) hydrochloride (HAMA) was synthesized by grafting the AEMA group on an HA polymer and served as the control (Ctrl) group without the DA group. The peaks from 6.5 to 7.2 parts per million (ppm) in the HAD ^{1}H nuclear magnetic resonance (NMR) spectra indicated the protons in the catechol ring of the DA group. The peaks at 5.68 and 6.13 ppm were assigned to the C═C bond protons of the AEMA group (Fig. 2B and fig. S1, A to C). In addition, compared with the Fourier transform infrared (FTIR) spectra of the HA polymer, the synthetic HAD and HAMA polymers both showed the wave number of 1633 cm^{-1} that was assigned to the C═C bond in the AEMA group (fig. S1D). Moreover, HAD samples showed an increase in the intensity of the ─OH group peak at about 3360 cm^{-1} formed by the graft of the catechol groups compared with HAMA samples. Therefore, the ^{1}H NMR and FTIR analysis results both confirmed that the AEMA and DA groups were successfully grafted onto the HA polymer chains in HAD polymer. Rheological tests of HAD precursor subjected to different shear rates confirmed that its shear thinning capacity resembled those of HAMA (HA polymer grafting with AEMA group) and HA polymer solution (Fig. 2C). The HAD precursor exhibited lower viscosity than that of the HA solution but higher than that of HAMA. The hydroxyl moiety in the DA group maintained hydrogen interactions and resulted in the same viscosity level as that of HA. Overall, the HAD precursor would be injectable because of its shear thinning property. The HAD hydrogel was then formed after photocrosslinking aqueous HAD precursor solution in the presence of a lithium phenyl(2,4,6-trimethylbenzoyl) phosphinate (LAP) photoinitiator under ultraviolet (UV) irradiation (365 nm) for 15 s (Fig. 2D). The porous microarchitecture of the lyophilized HAD hydrogel was confirmed under a scanning electron microscope (SEM) (Fig. 2D). The mechanical properties of the hydrogels were investigated in a rheological study. The frequency sweep test showed that all of these samples showed a higher storage modulus (G') than loss modulus (G'') in the frequency ranging from 0.1 to 10 Hz, which suggests their good gelation network after photocrosslinking. Especially, the G' of HAD hydrogel was slightly lower than that of HAMA hydrogel because of the hydrophilicity of catechol groups in HAD (Fig. 2E). In addition, the HAD hydrogels reached equilibrium swelling with about 380% after soaking for 4500 min (3 days), while the HAMA hydrogel showed an equilibrium swelling ratio of only about 100% (fig. S2A). These results also indicated that the hydrophilicity of catechol groups in HAD hydrogels contributed to their swelling behavior. HAD precursor solution was pipetted onto the surface of the pig heart to evaluate the adhesive properties of HAD in heart tissue. The photocrosslinked HAD hydrogel adhered to the heart surface, and running water did not rinse it off (Fig. 2F and movie S1). Good adhesion of HAD hydrogel would maintain its integrity in response to friction with the other organs in the thoracic cavity. The HAD hydrogel swollen in phosphate-buffered saline (PBS) for 24 hours also maintained good adhesion on the heart surface (fig. S3 and movie S1). Hence, HAD would still adhere to the heart tissue even after swelling in the thoracic fluid. The good adhesion of HAD is explained by the strong interactions between the catechol groups of HAD and the natural nucleophiles (amino bonds, thiols, and amines) in the proteins on the heart tissue surface (Fig. 2G). Stabbed, stretched, twisted, and bent HAD hydrogel maintained its stability and integrity on the heart tissue crack sites (Fig. 2H). Furthermore, HAD hydrogel stopped cardiac bleeding. A deep wound to the heart caused blood leakage and pale red semiopaque coloration in the ambient liquid environment. However, HAD hydrogel sealing stopped the blood leakage from the heart wound and restored the ambient liquid to its natural clear, colorless, transparent state (Fig. 2I and movie S2). On the other hand, the degradation properties in vitro of HAD hydrogel were also studied by measuring the dry weights of the hydrogels for 4 weeks. The result showed that about 22% weight of HAD hydrogel and 24% weight of HAMA hydrogel degraded after incubating in PBS (pH 7.4) for 4 weeks (fig. S2B). Furthermore, we also evaluated the biocompatibility of HAD hydrogel in vitro. As shown in fig. S4, very few dead cells (red fluorescence) were observed in both the HAD group and the Ctrl group on day 1 and day 3. The statistical results demonstrated that there was no significant difference in cell viability between the HAD group and the Ctrl group, which indicated the good biocompatibility of our HAD hydrogel.

HAD hydrogel exhibited asymmetric adhesion, which was controlled by photocrosslinking. Figure 2F shows that the HAD precursor adhered to the pig heart tissue because of the strong interactions between its catechol groups and the natural nucleophiles in the proteins on the heart tissue surface. The outside surface of the photocrosslinked HAD hydrogel demonstrated antiadhesion behavior because the cross-linked AEMA network restricted the movement of the catechol groups and prevented them from interacting with the heart surface nucleophiles (sol-adhesive process) (Fig. 3A). In contrast, when the HAD precursor was photocrosslinked before it was applied to the heart tissue surface, the HAD hydrogel failed to adhere because the movement of the catechol groups was restricted (gel-nonadhesive process) (Fig. 3B). Lap shear tests were used to evaluate the asymmetric adhesiveness of HAD hydrogel and measure the strength of its adhesion to the heart tissue under the sol-adhesive and gel-nonadhesive processes. The heart tissue was

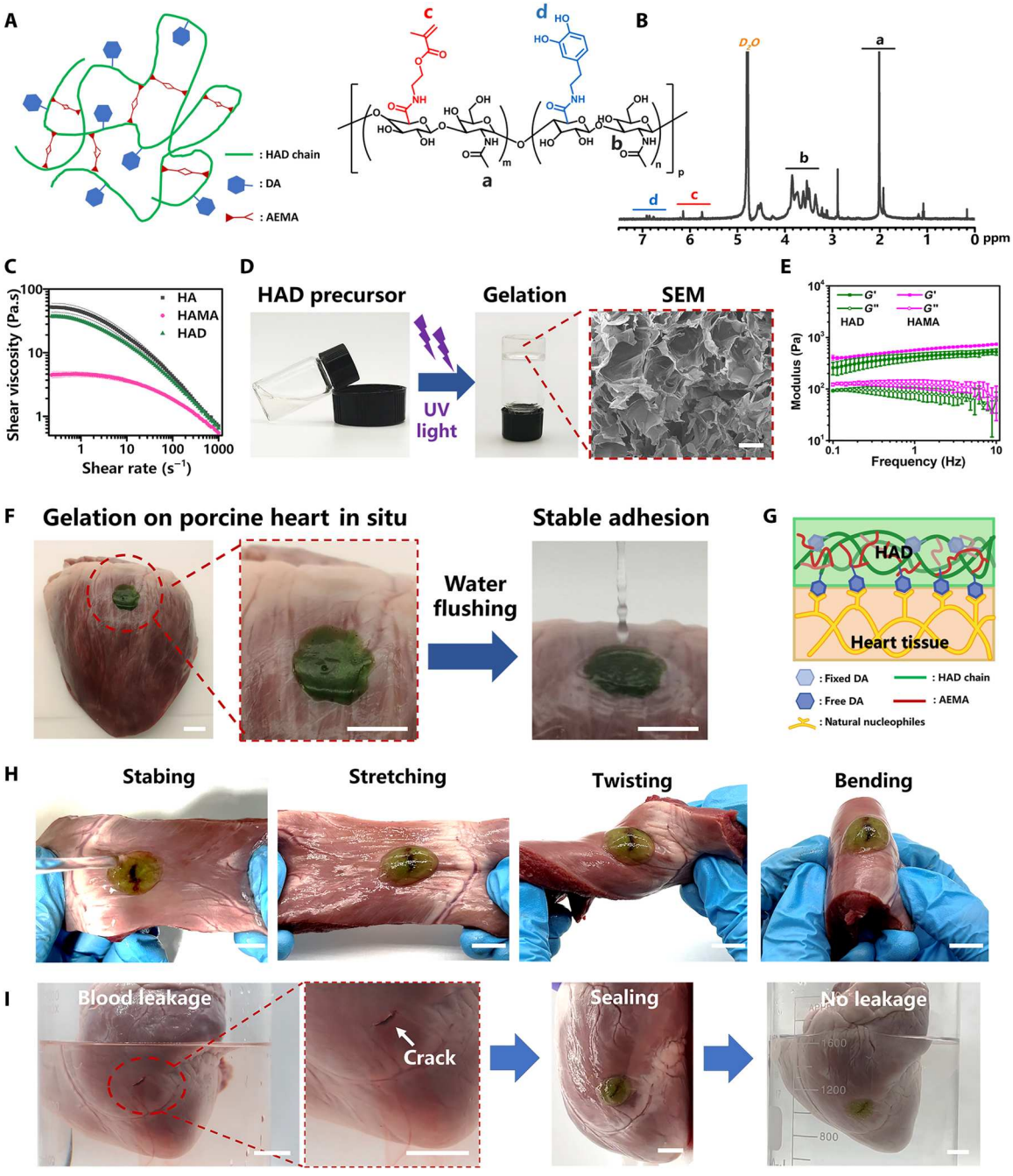

Fig. 2. Characterization of HAD hydrogel. (**A**) Molecular structure of HAD hydrogel. (**B**) ^{1}H NMR spectra of HAD. "a" corresponds to the C(═O)CH3 in HA (δ = 2.1 ppm), "b" corresponds to the protons in the ring structures of HA (δ = 4.0 to 3.0 ppm), "c" corresponds to the C═C of AEMA (δ = 5.68 and 6.13 ppm), and "d" corresponds to the protons in the catechol ring of DA (δ = 6.5 to 7.2 ppm). (**C**) Rheological viscosity test of HAD, HAMA, and HA under different shear rates. (**D**) Hydrogels were UV-irradiated and then photocrosslinked. Scale bar, 300 μm. (**E**) The mechanical property of HAD and HAMA hydrogel (n = 3 per group). (**F**) In situ HAD hydrogel adhesion to pig heart was stable after water rinsing. Scale bars, 1 cm. (**G**) Schematic diagram of HAD hydrogel adhesion to heart tissue. (**H**) After stabbing, stretching, twisting, and bending, HAD hydrogel maintained its stability and integrity on the heart tissue crack site. Scale bars, 1 cm. (**I**) HAD hydrogel sealed heart crack and prevented blood leakage from it. Scale bars, 1 cm.

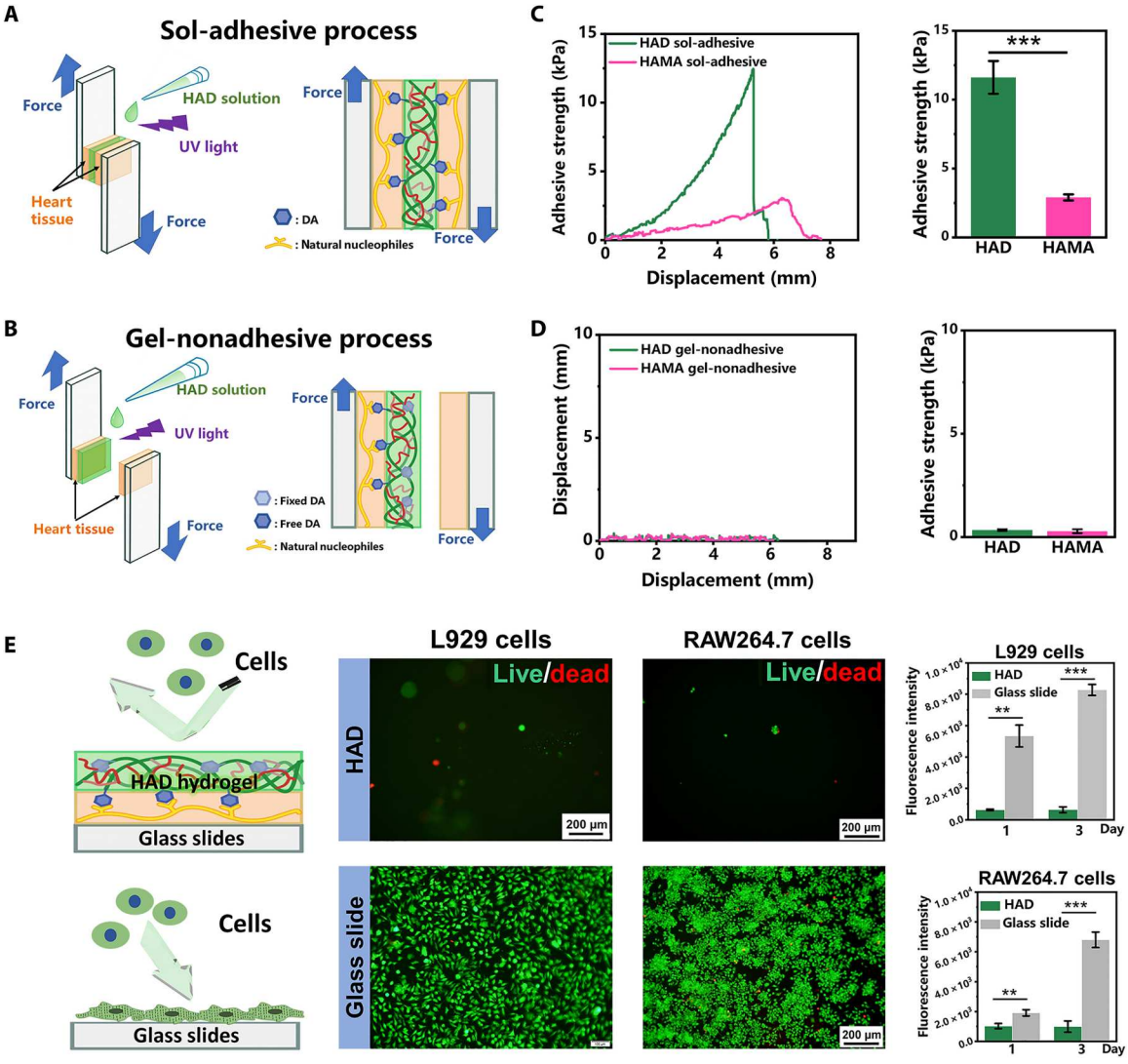

Fig. 3. Asymmetric adhesiveness in HAD hydrogel. (**A** to **D**) Schemes showing "sol-adhesive" (A) and "gel-nonadhesive" properties of HAD hydrogel (B) and strength of adhesion between HAD or HAMA hydrogel and pig heart tissue following sol-adhesive process (C) and gel-nonadhesive process (D) (n = 4 per group). (**E**) L929 and RAW264.7 cell adhesion on HAD hydrogel and glass slides (Ctrl). $^{**}P < 0.001$ and $^{***}P < 0.0001$.

cut into 15 mm by 30 mm by 6 mm pieces that were used in the subsequent tests (fig. S5). Under the sol-adhesive process, HAD hydrogel had significantly higher adhesive strength (11.62 ± 1.19 kPa) than HAMA hydrogel (2.89 ± 0.22 kPa) ($P < 0.01$) (Fig. 3C and movie S3). The HAD hydrogel had numerous free catechol groups that strongly interacted with the natural nucleophiles in the proteins on the heart surface. In contrast, the HAMA hydrogel lacked sufficient moieties that could adhere to the heart tissue. HAD hydrogel also had greater adhesion strength than a commercial fibrin glue. (*26*) Under the gel-nonadhesive process, both the HAD and HAMA hydrogels exhibited very low adhesive strength (<0.33 kPa) (Fig. 3D). The lap shear test results demonstrated that the HAD hydrogel had asymmetric adhesiveness because of photocrosslinking and catechol group (DA) grafting. Fibroblasts and macrophages are recruited by the immune system to promote postoperative adhesion (*27*, *28*). We evaluate the in vitro antiadhesion capacity of HAD using L929 fibroblasts and RAW264.7 macrophages, which are commonly implicated in postoperative adhesions. The cells were seeded onto the surface of the HAD hydrogel. Cells mounted on glass slides served as the Ctrl. Live/dead staining revealed very few round cells on the HAD hydrogel surface but abundant, widely spread cells adhering to the glass slides (Fig. 3E). The cell proliferation assay confirmed that the few L929 fibroblasts and RAW264.7 macrophages adhering to the HAD hydrogel surface did not proliferate during 3 days of cultivation. In contrast, the same cells normally proliferated on the glass slides (fig. S6). The polyanion HA inhibits attachment and spreading in most mammalian cells as its negatively charged surface repels negatively charged cell membranes (*29*). The DA groups provide cell adhesion sites. In the photocrosslinked HAD hydrogel, however, they were fixed inside the network where they could not promote cell adhesion. As HAD hydrogel resists cell adhesion, it could also potentially inhibit adhesion after cardiac surgery.

We differentiated human induced pluripotent stem cells (hiPSC) cells into hiPSC-CMs according to a previously reported protocol (*30*). After differentiation, flow cytometry results showed 92.59% of iPSC-CMs were positive for cardiac troponin T (cTnT), which suggested the high differentiation efficiency of iPSC (fig. S7A). Immunofluorescence images also showed positive expression of α-sarcomeric actin and cTnT (fig. S7B). Exosomes were derived from the hiPS-CM culture medium, designated iCM-EXOs, and characterized by transmission electron microscopy (TEM), nanoparticle tracking analysis (NTA), and Zetasizer Nano analysis. The iCM-EXOs displayed typical "cup rim" morphology under TEM (Fig. 4A). The NTA indicated that the average and range of the iCM-EXO diameters were 91 nm and 70 to 125 nm, respectively (Fig. 4B). The iCM-EXOs had negative zeta potential (−16.7 mV) (Fig. 4C) and were, therefore, stable. Western blotting confirmed the presence of the exosome-specific markers CD9, CD63, Syntenin, and Alix in the iCM-EXOs (Fig. 4D). Fluorescence imaging verified the capacity of CMs to absorb iCM-EXOs (fig. S8). When the primary cardiomyocytes were cultured with PKH26-labeled iCM-EXOs, the former acquired red fluorescence, which means that they absorbed the labeled iCM-EXOs. The preceding results validated the successful preparation and absorption of iCM-EXOs derived from hiPS-CMs.

We treated primary cardiomyocytes with PBS, H_2O_2, and H_2O_2 in the presence of iCM-EXOs, respectively, and used annexin V–fluorescein isothiocyanate (FITC) and propidium iodide (PI) staining to assess apoptosis. Flow cytometry confirmed that >46.9% of all cells were apoptotic after H_2O_2 treatment (H_2O_2 group), whereas only 11.8% of all cells were apoptotic in the absence of H_2O_2 (Ctrl). In the presence of iCM-EXOs plus H_2O_2 (H_2O_2 + iCM-EXOs group), only 33.9% of the cells were apoptotic. This apoptosis rate was significantly lower than that for the cells subjected to H_2O_2 alone ($P < 0.01$) (Fig. 4, E and F). A cell counting kit-8 (CCK-8) assay showed that the viability of the H_2O_2 + iCM-EXOs group was higher than that of the H_2O_2 group (Fig. 4G). Hence, iCM-EXOs may protect cells against apoptosis that occurs after H_2O_2 treatment. We then investigated the effects of iCM-EXOs on oxidative stress in primary cardiomyocytes. The stain 2′,7′-dichlorofluorescein (DCF) discloses ROS generation. DCF staining images, quantitative statistical analysis, and flow cytometry revealed that the iCM-EXO treatment significantly decreased ROS generation in H_2O_2-stimulated CMs (Fig. 4, H and I, and fig. S9A). JC-1 staining probes the changes that occur in primary cardiomyocyte mitochondria after H_2O_2 treatment. JC-1 is a fluorescent lipophilic carbocyanine dye that is used to visualize the mitochondrial membrane potential (Δψm or MMP). Green and red fluorescence indicate low and high MMP, respectively. Figure 4J reveals that relatively more cells fluoresced red in the Ctrl and H_2O_2 + iCM-EXOs groups, while comparatively more cells fluoresced green in the H_2O_2 group. The red:green fluorescence ratio was significantly higher for the H_2O_2 + iCM-EXOs group than the H_2O_2 group (Fig. 4K). Moreover, the flow cytometry of MMP also showed the same trend (fig. S9B). Therefore, iCM-EXOs may hinder oxidative stress–induced perturbation of the MMP.

We detected the protein expression of nuclear factor erythroid 2–related factor 2 (Nrf2), Kelch-like ECH-associated protein-1 (Keap1), reduced form of nicotinamide adenine dinucleotide phosphate quinone oxidoreductase 1(NQO1), and heme oxygenase 1 (HO-1) via Western blotting to clarify the molecular mechanism by which iCM-EXOs protect against H_2O_2-induced oxidative damage. The cytoplasmic Nrf2 levels were lower and the NQO1 and HO-1 levels were higher in the H_2O_2 group than in the Ctrl group (Fig. 4, L and M). In contrast, the iCM-EXO treatment significantly inhibited the decrease in cytoplasmic Nrf2 protein and the increases in NQO1 and HO-1 in H_2O_2-treated cardiomyocytes. The expression of Keap1 in each group showed no significant difference ($P > 0.05$), which suggests that Keap1 undergoes a conformational change rather than changes in expressions related to the expression of Nrf2 (fig. S10). The preceding results suggest that iCM-EXOs inhibit Nrf2 activation, attenuate oxidative stress in primary cardiomyocytes in vitro, and have potential antioxidant efficacy in vivo.

The iCM-EXOs were resuspended in HAD precursor solution to load them into the HAD hydrogel. After photocrosslinking, the iCM-EXOs were encapsulated within the HAD hydrogel, and the product was designated the HAD+EXOs hydrogel. The iCM-EXOs were prelabeled with PKH26, and the HAD hydrogel was mixed with FITC to visualize the iCM-EXOs within the HAD hydrogel. Fluorescence images disclosed that the PKH26-labeled iCM-EXOs were uniformly distributed within the hydrogel (Fig. 5A). The three-dimensional (3D) views of the fluorescence images confirmed the homogeneous distribution of iCM-EXOs within the HAD+EXOs hydrogel (Fig. 5B). Fluorescence intensity analysis of the HAD+EXOs hydrogel cross section revealed good longitudinal and lateral iCM-EXO distribution (Fig. 5C). Furthermore, with the encapsulation of iCM-EXOs, HAD+EXO hydrogel showed no significant difference from HAD hydrogel in terms of storage modulus ($P > 0.05$) (fig. S11). The HAD+EXOs were immersed in PBS at 37°C for 15 days to simulate sustained in vivo release of iCM-EXOs. The latter was detected with a micro–bicinchoninic acid (BCA) protein assay kit (Thermo Fisher Scientific, Chengdu, Sichuan, China) according to the manufacturer′s instructions. The standard curve for the iCM-EXOs is shown in fig. S12. The iCM-EXOs were very rapidly released from the HAMA+EXOs hydrogel. By day 7, 83.2% of all iCM-EXOs had been released. In contrast, only 58.0% of the iCM-EXOs had been released from the HAD+EXOs hydrogel by day 7. The sustained release of iCM-EXOs from the HAMA+EXOs hydrogel reached its upper limit of 95.2% by day 11. However, only 89.9% of the iCM-EXOs had been released from the HAD+EXOs hydrogel by day 13 (Fig. 5D). The foregoing results demonstrated the satisfactory sustained release behavior of HAD+EXOs hydrogel and the potential capacity of HAD hydrogel to deliver exosomes.

Figure 6A shows that part of the pericardium was excised to release the pericardial fluid and expose the epicardium. The latter was then stabbed 100 times with a needle to induce bleeding. This approach simulated the post–cardiac surgery condition characterized by incomplete pericardium, pericardial fluid leakage, autogenous bleeding followed by acute inflammation and oxidative stress, and chronic pericardial adhesion. HAD or HAD+EXOs precursor solutions were applied to the bleeding sites in the epicardium. The photocrosslinked HAD and HAD+EXOs hydrogels fully covered the target sites (Fig. 6A). We then labeled the hydrogel precursor with indocyanine green (ICG) to visualize it under near-infrared (NIR) light and measure the HAD+EXOs and HAD hydrogel retention times on the heart surface. The first week after heart surgery is the acute period when oxidative stress and immunoreactions may occur. At that time, the HAD and HAD+EXOs hydrogels induced

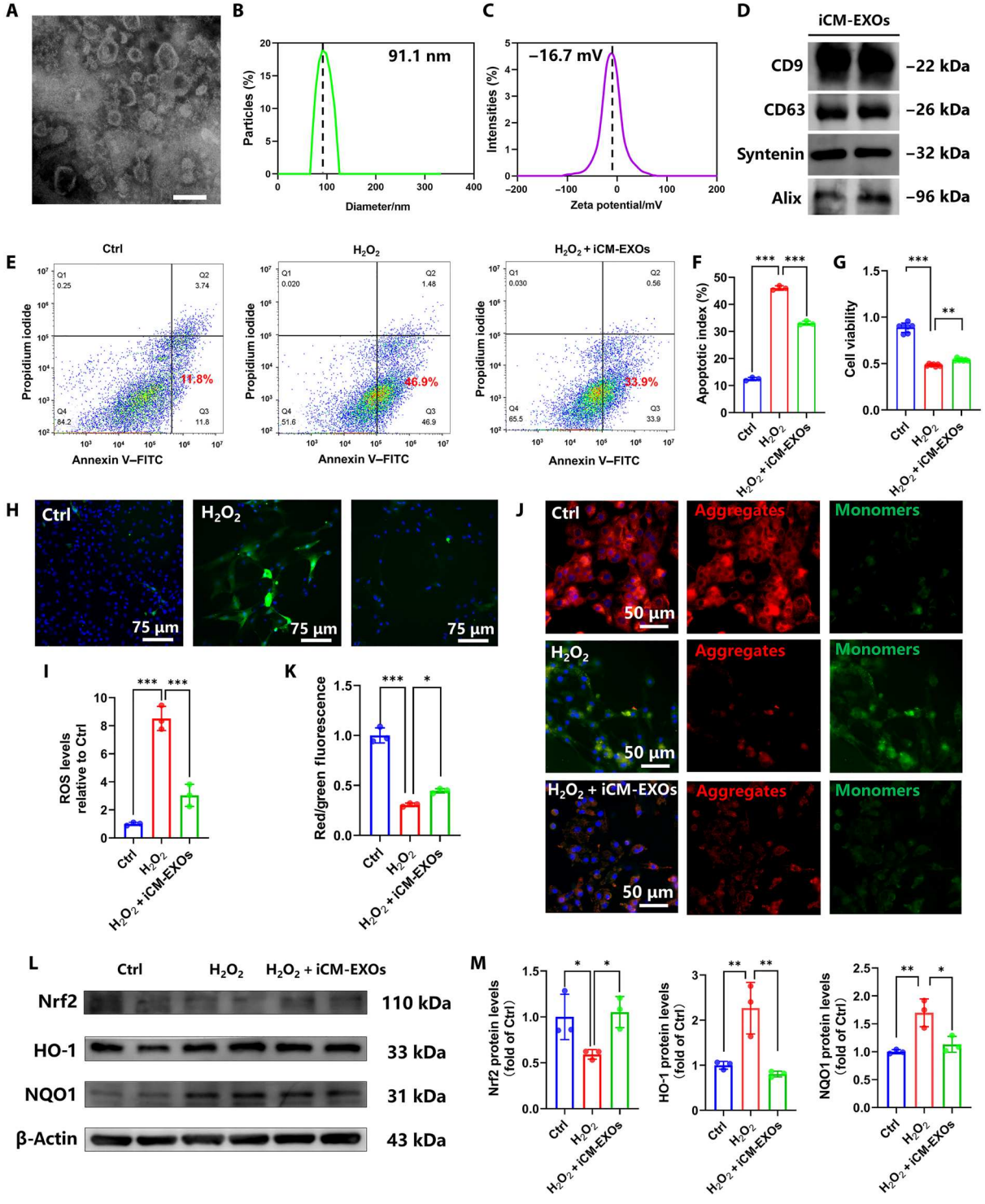

Fig. 4. iCM-EXOs inhibit oxidative stress and ameliorate mitochondrial changes in H_2O_2-stimulated CMs. (**A**) TEM image of iCM-EXOs. Scale bar, 200 μm. (**B**) Size distributions of isolated iCM-EXOs determined by NTA. (**C**) Negative zeta potentials of iCM-EXOs. (**D**) Western blots of exosome-specific marker protein expression in iCM-EXOs. (**E** and **F**) Flow cytometry of apoptotic cells in each group ($n = 4$). (**G**) Cell viability of primary cardiomyocytes in each group ($n = 4$). (**H** and **I**) Representative DCF (green) and 4′,6-diamidino-2-phenylindole (blue) staining images revealing ROS generation. Histogram showing ROS level compared with that of the Ctrl group ($n = 4$ per group). (**J** and **K**) JC-1 staining showing representative images of MMP. Green fluorescence is the monomeric JC-1 that forms in cytosol. Red fluorescence is the potential-dependent aggregation in the mitochondria of each group. Histogram showing red:green JC-1 fluorescence in each group ($n = 4$ per group). (**L** and **M**) Western blots and histograms of Nrf2, HO-1, and NQO1 in primary cardiomyocytes of each group. $^*P < 0.05$, $^{**}P < 0.001$, and $^{***}P < 0.0001$.

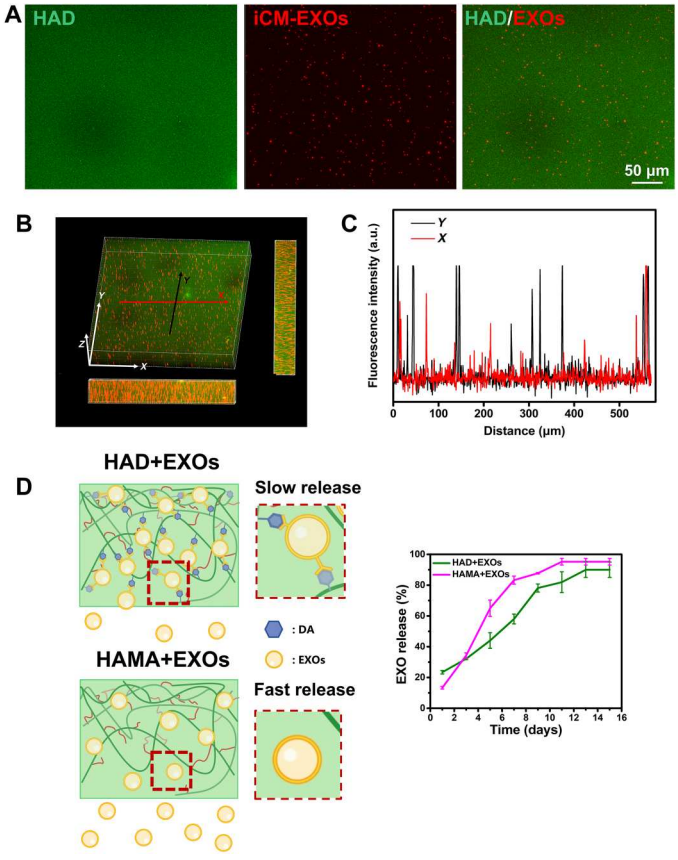

Fig. 5. Sustained release behavior of HAD+EXOs hydrogel. (**A**) Fluorescence images showing iCM-EXOs (red; labeled with PKH26) encapsulated within HAD hydrogels (green; labeled with FITC). (**B** and **C**) 3D views of confocal HAD+EXOs hydrogel images and fluorescence intensity analysis of their cross sections revealing the homogeneous iCM-EXO distribution within HAD+EXOs hydrogel. (**D**) Schematic diagram of iCM-EXO release from HAD+EXOs and HAMA+EXOs hydrogels and graph plotting sustained release over 15 days (n = 4 per group).

intense signals in the heart at the thoracotomy (suturing) site (Fig. 6B). Two weeks after heart surgery, the HAD hydrogel and HAD+EXOs hydrogel signals had declined to levels below NIR (Fig. 6C). There was no significant difference in retention time between the HAD and HAD+EXOs hydrogels. Hence, iCM-EXO encapsulation had no impact on the HAD+EXOs hydrogel retention time in vivo. We also measured the superoxide dismutase (SOD) and glutathione (GSH) levels 7 days after heart surgery. As the HAD+EXOs hydrogel provided sustained iCM-EXO release, the HAD+EXOs group secreted relatively larger amounts of SOD and GSH than the HAD and model groups in response to oxidative challenge in vivo (Fig. 6, D and E). We then used enzyme-linked immunosorbent assay (ELISA) and quantitative polymerase chain reaction (qPCR) to measure the gene and protein expression levels of the proinflammatory cytokines interleukin-1β (IL-1β), tumor necrosis factor–α (TNF-α), and IL-6. HAD hydrogel significantly ($P < 0.05$) and HAD+EXOs hydrogel very significantly ($P < 0.001$) down-regulated all three cytokines compared with the model group (Fig. 6, F and G). These results suggest that the sustained iCM-EXO release provided by HAD+EXOs hydrogel was both antioxidant and anti-inflammatory after cardiac surgery (Fig. 6H).

We compared pericardial adhesion in the HAD+EXOs hydrogel, iCM-EXOs, HAD hydrogel, and model groups at 2 weeks after cardiac surgery. A gross examination of pericardial adhesion formation was conducted after the thoracic cavities were reopened. Representative images of the harvested postoperative hearts are shown in Fig. 7A. Each heart was divided into nine sections, and the overall severity of adhesion in each section was rated on a scale of 0 to 4 (Fig. 7B). The model and iCM-EXO groups did not significantly differ in terms of the three scores mentioned previously. Thus, inhibiting oxidative stress by exosome administration did not prevent pericardial adhesion in vivo. In contrast, postoperative adhesions were significantly reduced in the HAD and HAD+EXOs groups compared with the model group (Fig. 7C). The average adhesion intensity scores of the HAD (0.94 ± 0.68) and HAD+EXOs (0.39 ± 0.42) groups were lower than that of the model group (1.83 ± 0.72). The average adhesion scores of the HAD (0.54 ± 0.52) and HAD+EXOs (0.15 ± 0.22) groups were also lower than that of the model group (1.44 ± 1.04). Hematoxylin and eosin (H&E) staining disclosed abundant fibrous tissue and severe adhesion on the surfaces of the hearts in the model and iCM-EXO groups. By contrast, only sparse fibrous tissues were detected on the surfaces of the hearts in the HAD and HAD+EXOs groups (Fig. 7D). About 4.73 ± 1.2% and 3.03 ± 0.43% fibrous tissue was on the surfaces of the postoperative heart in the HAD and HAD+EXOs groups, respectively. On the other hand, 22.23 ± 4.04% and 20.93 ± 1.04% fibrous tissue was on the surfaces of the postoperative heart in the model and iCM-EXOs groups, respectively (Fig. 7E). In the present study, only a few $GATA^{6+}$ macrophages (red) were observed at the adhesive side of the HAD+EXOs group, whereas numerous $GATA^{6+}$ macrophages were recruited to the adhesive side of the model group at 1 week after surgery. Macrophage scavenger receptor-1 (MSR-1; positive charge) was abundant in the peripheral region of the adhesive sites in the model group (Fig. 7, F and G). Thus, $GATA^{6+}$ macrophages were recruited to the sites and contributed to postoperative adhesion. In contrast, very little MSR-1 was detected at the adhesive sites of the HAD+EXOs group. The preceding results demonstrated that HAD+EXOs hydrogel may prevent postoperative adhesions in a rat cardiac surgery model by suppressing the recruitment of $GATA^{6+}$ cavity macrophages to the adhesion sites.

Postoperative adhesion was assessed at 4 weeks after heart surgery to evaluate the long-term efficacies of the HAD, iCM-EXOs, and HAD+EXOs treatments relative to the untreated model. The gross assessment of reductions in the formation of postoperative adhesions is shown in Fig. 8A. The HAD and HAD+EXOs groups presented with inconspicuous adhesion, whereas the model and iCM-EXOs groups displayed obvious adhesion. H&E staining images revealed different degrees of adhesion on the surfaces of the postoperative hearts from each group. The model and iCM-EXOs groups exhibited abundant fibrous tissue and severe adhesion on their heart surfaces, whereas only sparse fibrous tissue was observed on the surfaces of the hearts from the HAD and HAD+EXOs groups (Fig. 8A). For all treatment groups, the average adhesion and adhesion intensity scores and the maximum adhesion intensities were lower at 4 weeks after surgery than they were at 2 weeks after surgery. Nevertheless, the adhesion scores still significantly differed among treatment groups. The HAD+EXOs and HAD groups had lower average adhesion intensities (0.07 ± 0.19 and 0.36 ± 0.38, respectively) than the model and iCM-EXOs groups (1.07 ± 0.80 and

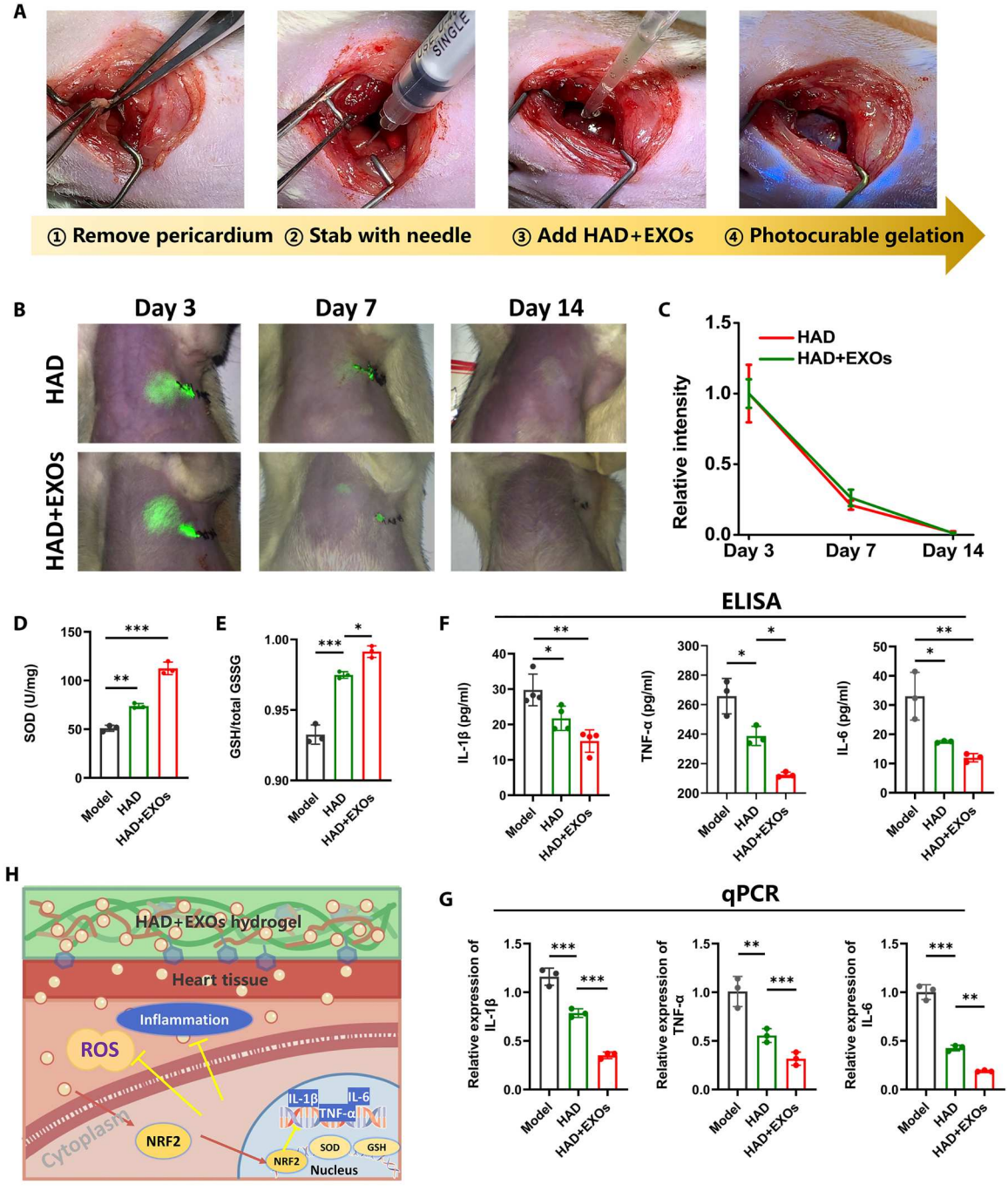

Fig. 6. HAD+EXOs reduced oxidative stress and immunoreactions in a rat post-cardiac surgery model. (**A**) Establishment of a rat pericardial adhesion model. (**B** and **C**) Fluorescence images and in vivo retention times of HAD and HAD+EXOs hydrogels in rat hearts on days 3, 7, and 14 after cardiac surgery ($n = 3$ per group). (**D**) Cardiac SOD levels 1 week after cardiac surgery ($n = 4$ per group). (**E**) GSH:Glutathione oxidized (GSSG) ratios in the heart tissue at 1 week after cardiac surgery ($n = 4$ per group). (**F**) ELISA of IL-1β, TNF-α, and IL-6 at 1 week after cardiac surgery ($n = 4$ per group). (**G**) qPCR of relative *IL-1β*, *TNF-α*, and *IL-6* expression at 1 week after cardiac surgery ($n = 4$ per group). (**H**) Antioxidant and anti-inflammatory mechanisms of HAD+EXOs hydrogel after cardiac surgery. $^{*}P < 0.05$, $^{**}P < 0.001$, and $^{***}P < 0.0001$.

0.86 ± 0.85, respectively). The average adhesion scores and maximum adhesion intensities showed similar trends (Fig. 8B). The foregoing results indicated that both the HAD and HAD+EXOs treatments maintained long-acting antiadhesion efficacy after heart surgery. We performed M-mode echocardiography to evaluate the systolic and diastolic functions of the heart at 4 weeks after surgery (Fig. 8C). In our study, the needling method can induce bleeding and postoperative adhesion without impact on cardiac function (*9*), so the sham group and model group showed no statistical difference. Moreover, the treatment and model groups did not significantly differ in terms of ejection fraction, fractional shortening, end-systolic left ventricular internal diameter

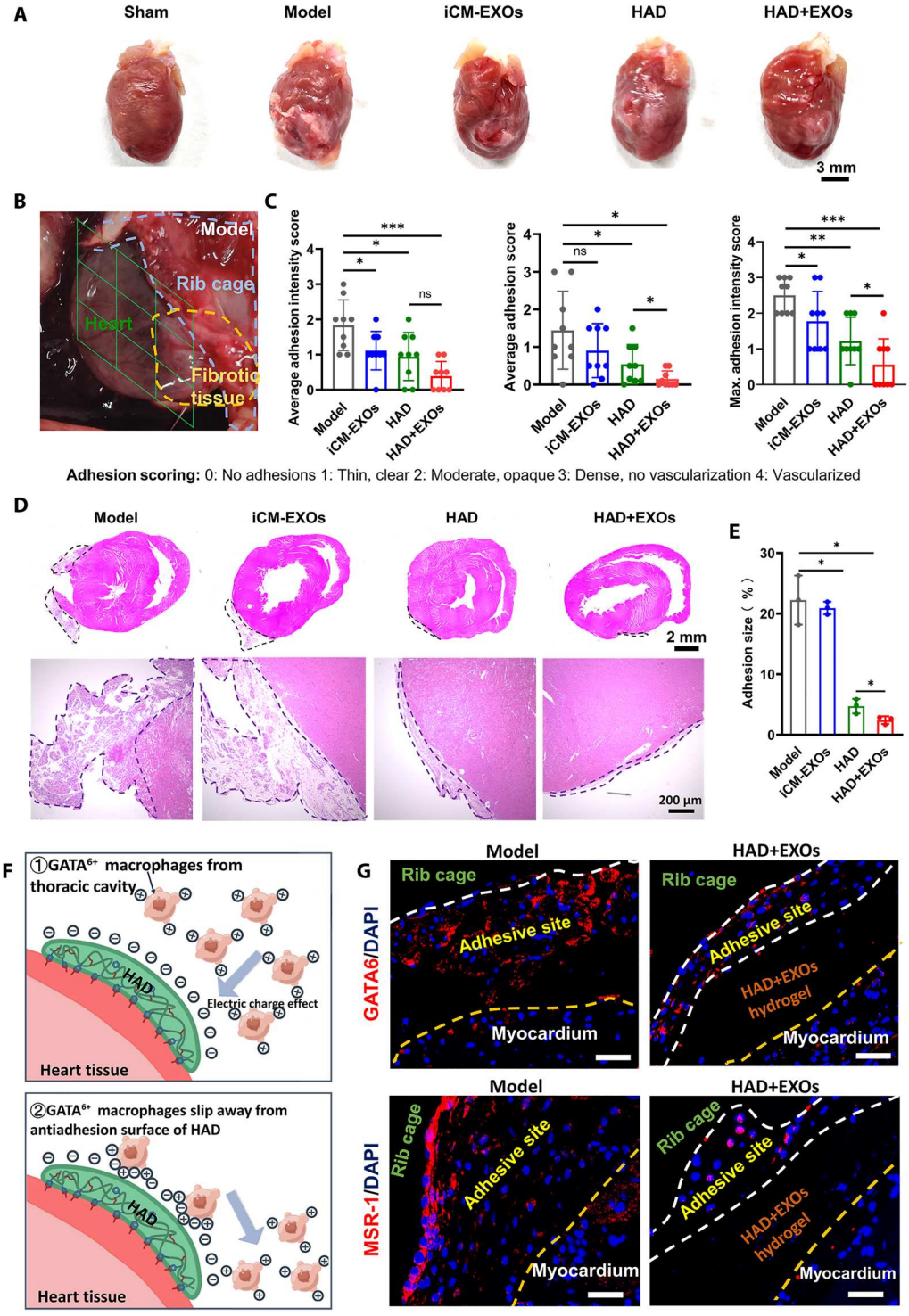

Fig. 7. HAD+EXOs reduced postoperative adhesion after 2 weeks in a rat post–cardiac surgery model. (**A**) Representative gross images of postoperative hearts from the model, iCM-EXOs, HAD, and HAD+EXOs groups. (**B**) Representative images of the model group. Hearts were divided into nine sections and their adhesion scores were evaluated. (**C**) Adhesion scores for each group ($n = 9$ per group). (**D**) Representative H&E staining images of rat hearts. (**E**) Sizes of adhesions (%) in rat hearts from each group ($n = 4$ per group). (**F**) Mechanism of the antiadhesion effect of HAD. (**G**) Immunofluorescence images showing $GATA^{6+}$ (red) and MSR-1 (red) in the model and HAD+EXOs groups. *$P < 0.05$, **$P < 0.001$, and ***$P < 0.0001$. ns, no significant difference.

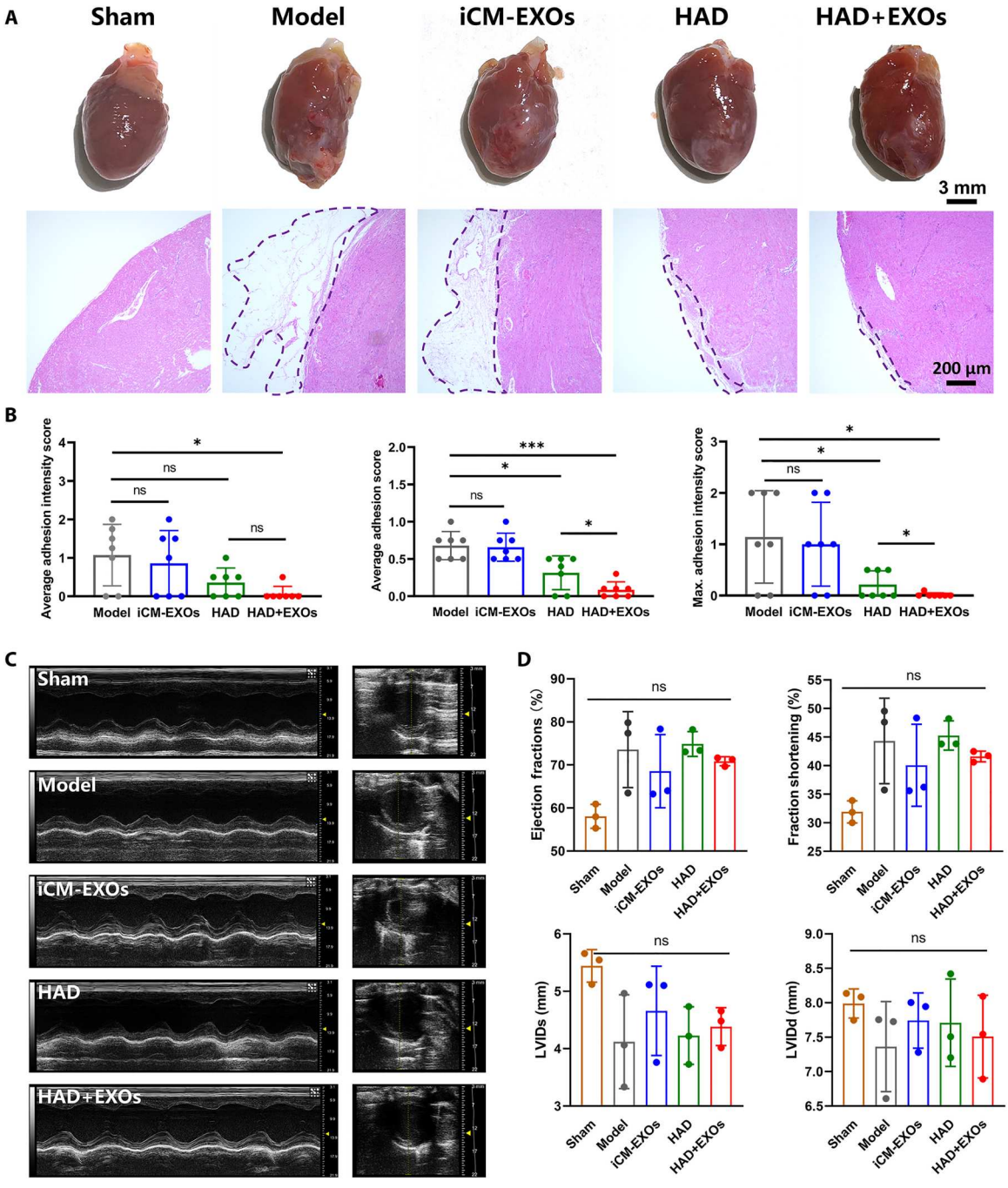

Fig. 8. HAD+EXOs reduced postoperative adhesion and maintained cardiac function at 4 weeks after rat heart surgery. (**A**) Representative gross images of postoperative hearts from the model, iCM-EXOs, HAD, and HAD+EXOs groups. (**B**) Adhesion scores for each group ($n = 7$ per group). (**C**) Representative H&E staining images of rat hearts. (**D** and **E**) Representative M-mode images and ejection fraction, fraction shortening, LVIDs, and LVIDd values determined by echocardiography of the model, iCM-EXOs, and HAD+EXOs groups at 4 weeks after surgery ($n = 3$ per group). *$P < 0.05$ and ***$P < 0.0001$.

(LVIDs), or end-diastolic left ventricular internal diameter (LVIDd). Hence, cardiac function remained normal following HAD+EXOs hydrogel application (Fig. 8D). Moreover, echocardiography demonstrated that HAD+EXOs had no significant impact on cardiac function.

DISCUSSION

In the present study, we successfully designed and synthesized a Janus hydrogel with asymmetric adhesive properties. The inspiration for the hydrogel design was mussel grafting catechol groups. HA was selected as the principal polymer chain. Commercial Na-HA solution washout has been applied to limit adhesion during cardiac surgery. Nevertheless, this approach had limited efficacy

because of its very short retention time. A prior investigation cross-linked HA to improve its mechanical properties and extend its retention time (*31*, *32*). Here, we grafted DA and AEMA onto the HA chain to functionalize it with adhesiveness and photocrosslinking, respectively (Fig. 2A). DA mediates the formation of mussel adhesives and has recently been used widely in the design of adhesive materials (*9*, *33*, *34*).

For the "sol-adhesive" process as shown in Fig. 3A, the HAD precursor was first pipetted and adhered on the pig heart tissue, because of the Schiff base reaction or Michael addition reaction between the catechol groups in the HAD precursor and the natural nucleophiles (amido bonds, thiols, and amines) of the proteins on the heart tissue surface. Subsequently, the HAD hydrogel was then formed after photocrosslinking, which showed the antiadhesion behavior because the cross-linked AEMA network in the HAD hydrogel restricted the movement of the catechol groups and prevented them from interacting with the heart surface nucleophiles. Therefore, the key role of this asymmetric adhesive phenomenon is controlled by the photocrosslinking process, where the cross-linked AEMA network would restrict the movement of the catechol groups and prevent them from interacting with the heart surface nucleophiles. In contrast, for the "gel-nonadhesive" process, when HAD hydrogel was formed after photocrosslinking before it was applied to the heart tissue surface, the HAD hydrogel failed to adhere to the tissue surface because the movement of the catechol groups was restricted. The key role of this asymmetric adhesive phenomenon is controlled by the photocrosslinking process, where the cross-linked AEMA network would restrict the movement of the catechol groups and prevented them from interacting with the heart surface nucleophiles (Fig. 3C). During the process, the inside face of the HAD+EXOs hydrogel was able to adhere on the surface of the heart, while the opposite surface exhibited antiadhesion behavior, which we called the asymmetric adhesive properties. Furthermore, we used lap shear tests to evaluate the asymmetric adhesiveness of HAD hydrogel and measure the strength of adhesion between HAD hydrogel and pig heart under the sol-adhesive and gel-nonadhesive processes. The adhesive strength of HAD hydrogel was ~11.62 ± 1.19 kPa, surpassing that of commercial fibrin glue (*26*). HAD hydrogel could also stop cardiac bleeding in vitro. The in vitro model demonstrated that HAD hydrogel minimized or even prevented severe bleeding in isolated pig hearts (Fig. 2I). Hence, HAD hydrogel can effectively reduce pericardial adhesions as bleeding during cardiac surgery may result in severe postoperative adhesion. Blood and fibrin clots promote adhesion formation via fibrin accumulation. Thus, the pericardial cavity must be maintained free of blood and clots to prevent the formation of dense adhesions there (*4*).

In an earlier study on a rat model, exosomes were delivered to target sites via local multipoint or intravenous injection into the tail veins (*35*). However, these techniques had low delivery efficiency as exosomes can be rapidly cleared by macrophages and accumulate in other organs (*20*, *21*). Another study on a mouse model used Matrigel to suspend exosomes and improve exosome engraftment in the myocardium (*18*). However, Matrigel is not a strong adhesive and its retention time is very short. Therefore, its suitability for this application is critically limited. Here, we observed the sustained release of iCM-EXOs from HAD+EXOs hydrogel and their efficient delivery into the epicardium. At days 7 and 13 after surgery, 58.0 and 89.9% of the iCM-EXOs had been released from the HAD+EXOs hydrogel, respectively (Fig. 4D). In contrast, 83.2% of the iCM-EXOs had been released from the HAMA+EXOs hydrogel at day 7 after surgery. The sustained release of iCM-EXOs from HAMA+EXOs hydrogel had reached 95.2% of its capacity by day 11 after surgery. The presence of the catechol moieties in the HAD+EXOs hydrogel explains why it achieved a longer sustained release of iCM-EXOs than HAMA+EXOs hydrogel. HAD hydrogel is rich in DA, harboring catechol groups with a very high affinity for the natural nucleophiles (amido bonds and amines) on exosomes. For this reason, it requires relatively more energy to release the exosomes from the hydrogel. In contrast, HAMA hydrogel lacks catechol groups that can attract exosomes (Fig. 4D). The foregoing results demonstrated the sustained release behavior of HAD+EXOs hydrogel and the potential exosome delivery capacity of HAD hydrogel.

Patient-specific iPSC derivatives have been used to generate iCM-EXOs. The latter can be applied in autologous therapy as they activate endogenous repair. Preclinical studies have indicated that exosomes secreted from transplanted iPSCs and/or their derivatives improve heart function and stimulate angiogenesis by enhancing blood vessels and injured myocardium regeneration in the peri-infarcted area (*14*, *18*). Exosomes in dystrophin deficiency (Dys) iCMs protected the Dys-iCM from H_2O_2-induced injury by decreasing ROS production and release. In this way, the MMP was maintained (*36*). In the present study, iCM-EXOs protected primary cardiomyocytes subjected to H_2O_2 against apoptosis (Fig. 4E). Treatment with iCM-EXOs significantly reduced ROS generation and maintained the MMP in H_2O_2-stimulated CMs (Fig. 4, H to K). We also observed substantially higher cytoplasmic Nrf2 levels in the iCM-EXOs treatment than in the H_2O_2 treatment (Fig. 4L). Nrf2 is strongly associated with oxidative stress–mediated cardiac remodeling and heart failure (*37*, *38*). It is also a central player in cellular defense against oxidative stress and regulates downstream detoxifying enzymes and antioxidant proteins including NQO1, HO-1, SOD, and GSH. We observed NQO1 and HO-1 down-regulation (Fig. 4M) in response to iCM-EXOs treatment. Therefore, iCM-EXOs may inhibit Nrf2 activation, mitigate oxidative stress in primary cardiomyocytes in vitro, and have potential antioxidant efficacy in vivo. Our in vivo experiments revealed that the HAD+EXOs group (sustained iCM-EXO release) produced higher SOD and GSH as well as lower proinflammatory cytokine levels than the HAD and model groups at 1 week after cardiac surgery (Fig. 6, D and E).

Prior research disclosed that reducing oxidative stress and the inflammatory response with drugs could prevent postoperative pericardial adhesion in an animal model (*39*, *40*). The results of the present study showed that local exosome injection alleviated oxidative stress but failed to prevent pericardial adhesion in a rat post–cardiac surgery model. One possible explanation for this discrepancy is the fact that macrophages can eliminate injected exosomes (*21*). The HAD and HAD+EXOs groups presented with less fibrous tissue and adhesion than the model and iCM-EXOs groups. On the other hand, HAD hydrogel acted as a polyanion trap that inhibited $GATA^{6+}$ cavity macrophage recruitment by neutralizing the MSR-1 scavenger receptor and, by extension, preventing abdominal adhesion in vivo (*12*). HA is the main chain of HAD hydrogel. Because of the presence of carboxyl groups (COOH) in its molecular structure, HA has a negative charge. For the HAD hydrogel, although the addition of the DA and AEMA groups reacted with the part of COOH

groups on the HA chain (−57.3 ± 0.7 mV), the HAD still showed a negative zeta potential (−57.3 ± 0.7 mV) at pH 7.4 (*12*). Therefore, the surface of the HAD hydrogel showed a negative charge and had the capacity to attract the positive charge including MSR-1 on $GATA^{6+}$ macrophages (Fig. 7F). In the present study, only a few $GATA^{6+}$ macrophages were observed at the adhesive sites of the HAD+EXOs group, whereas numerous $GATA^{6+}$ macrophages were recruited to the adhesive sites of the model group at 1 week after surgery (Fig. 7G). The HAD group presented with inconspicuous adhesion compared to the model and iCM-EXOs groups. However, the HAD group had significantly higher average adhesion and maximum adhesion intensity scores as well as larger adhesions than the HAD+EXOs group (Fig. 7, B and C). The superiority of the HAD+EXOs hydrogel to the HAD hydrogel may be explained by the capacity of the former to encapsulate iCM-EXOs. HAD+EXOs hydrogel inhibited the recruitment of $GATA^{6+}$ cavity macrophages from the thoracic cavity and could, therefore, protect iCM-EXOs from macrophage clearance. The foregoing results confirmed that HAD hydrogel protects the iCM-EXOs from macrophage elimination, provides sustained iCM-EXOs release, and alleviates oxidative stress. They also indicate that HAD+EXOs inhibited pericardial adhesion to a greater extent than all other treatments as the HAD created a physical barrier and the iCM-EXOs were antioxidant.

At 4 weeks after surgery, the HAD+EXOs and HAD groups had lower average adhesion intensity scores (0.07 ± 0.19 and 0.36 ± 0.38, respectively) than the model and iCM-EXOs groups (1.07 ± 0.80 and 0.86 ± 0.85, respectively) (Fig. 8B). Therefore, both HAD and HAD+EXOs had prolonged postoperative adhesion prevention efficacy. M-mode echocardiography revealed that HAD+EXOs had no significant negative impact on normal, healthy cardiac function. In vivo, ICG labeling disclosed that most of the HAD and HAD+EXOs hydrogels degraded at 2 weeks after surgery. This retention time suffices to enable biodegradable barriers to prevent postoperative adhesion. The resorbable HA membrane Seprafilm has a 7-day retention time (*41*), while Coseal is completely resorbed within 30 days. Hence, there is a low risk that they will induce the inflammation and infection associated with permanently implanted or embedded foreign bodies.

Additional studies are necessary before this work can be translated clinically. First, the method of applying the HAD+EXOs hydrogel to the rat heart surface using syringes may not be practical for covering a larger area in a larger animal model in a short time, or for clinical applications in human surgery. Therefore, the development of a spray device to effectively spray the hydrogel and cover as much area as possible based on its shear thinning property may be explored. This would allow for more efficient and widespread application of the hydrogel. Second, in this study, a needling method was used to create a rat model to simulate post–heart surgery conditions, which is a commonly used method for preparing adhesion models (*9*, *42*). However, this model may not perfectly mimic the clinical status of the patients. In future large animal experiments, other models such as the cardiopulmonary bypass, aortotomy, valve replacement, or sternotomy models should be considered to investigate the clinical safety and efficacy validation of the HAD+EXOs hydrogel. These models induce more severe inflammatory responses compared to the needling methods, which may result in differences in postoperative adhesion scores and provide a more clinically relevant assessment. Last, in this study, exosomes were derived from hiPS-CMs via ultracentrifugation, which may result in batch-to-batch variance because of exosome heterogeneity. However, efforts are being made to establish good manufacturing practice (GMP) facilities for producing therapeutic exosomes, which can help manage the issue of batch-to-batch variance. Developing the HAD+EXOs hydrogel with GMP standards would be highly beneficial for future clinical translation of this work, as it would ensure consistent quality and safety of the hydrogel for clinical use.

The present work reported a HAD+EXOs hydrogel formulated by encapsulating iCM-EXOs in HAD hydrogels with asymmetric adhesiveness (fig. S13). The HAD+EXOs hydrogel has the potential efficacy at mitigating oxidative stress and reducing adhesion after cardiac surgery. One side of the UV-photocrosslinked HAD hydrogel facilitates adhesion to the wet myocardial surface, while its other side resists adhesion to the thoracic cavity. The antiadhesion side of HAD+EXOs hydrogel could inhibit the recruitment of $GATA^{6+}$ cavity macrophages from the thoracic cavity, thus protecting the iCM-EXOs from macrophages. On the other hand, the adhesion side of HAD+EXOs hydrogel could locally sustain the release iCM-EXOs to alleviate oxidative stress because of the high affinity of the catechol group and exosomes. The iCM-EXOs significantly attenuated oxidative stress in H_2O_2-treated primary cardiomyocytes in vitro by inhibiting Nrf2 activation. The HAD+EXOs hydrogel provided sustained release of its encapsulated iCM-EXOs for 15 days. In a rat post–cardiac surgery model, sustained iCM-EXOs release from the HAD+EXOs hydrogel alleviated oxidative stress and mitigated inflammation. HAD+EXOs hydrogel also significantly reduced pericardial adhesion in vivo and had no adverse effect on cardiac function. The HAD component contributed to the physical barrier while the iCM-EXOs had antioxidant efficacy. We believe that the HAD+EXOs hydrogel formulated, analyzed, and evaluated here is promising as an innovative clinical strategy for reducing postoperative pericardial adhesion.

MATERIALS AND METHODS

Materials

Sodium hyaluronate (molecular weight ~ 800 kDa) was purchased from Bloomage Biotech (China). Ethyl(dimethylaminopropyl) carbodiimide (EDC), *N*-hydroxysuccinimide (NHS), AEMA, and dopamine hydrochloride were purchased from Sigma-Aldrich and used without further purification (Shanghai, China). Dulbecco's PBS (DPBS; GIBCO), fetal bovine serum (FBS; GIBCO), and Live/Dead Viability Assay Kit and Alamar Blue (Molecular Probes) were used as received. hiPSC (U1 line) and differentiation media of hiPSC-CMs were purchased from Cellapy (Beijing, China).

Differentiation of hiPSCs into cardiomyocytes

Initially, hiPSC (U1 line) was seeded on growth factor reduced Matrigel (diluted 1:100) and cultured in Essential 8 medium. When the cells reached 80 to 90% confluence, they were passaged using hiPSC medium supplemented with 5 μM Y-27632 and incubated for 18 hours before being maintained in an iPS medium. Cardiomyocyte differentiation of hiPSC (hiPSC-CMs) was performed with a three-step method: Once the confluence of iPSC reached 50 to 80%, the culture medium was replaced by CM medium supplemented with 3 μM CHIR99021 for 48 hours, medium was changed into CM medium supplemented with 2 μM Wnt-C59 for 48 hours, and the cells were then maintained in CM medium for the following days.

Beating cells, indicative of cardiomyocyte differentiation, were observed between 7 and 8 days after the initiation of differentiation. Experiments were carried out once the proportion of beating cells reached 70 to 80%. For the replating of hiPSC-CMs, differentiated hiPSCs at days 9 to 21 were digested to seeded on a Matrigel-coated flask or plate cultured in a CM medium. The differentiation of hiPSCs into cardiomyocytes was induced by a reprogramming technique (*30*). Briefly, the hiPSCs were seeded on Matrigel (Corning)–precoated plates for 2 to 3 days under E8 media. When the cells′ confluence reached 70 to 80%, the medium was replaced with CM differentiation media I (D0). After 48 hours, the medium was replaced with CM differentiation media II (D2), and subsequently replaced with CM differentiation media III (D4). Last, beating cells are observed on day 9 after initiating reprogramming and further analyzed in the following days (days 18 to 22). To validate the differentiation of iPSC-CMs, flow cytometry was used to quantitatively detect the expression of cTnT using an LSR II analyzer (BD) and analyzed using FlowJo software.

Exosome isolation, identification, and uptake assessments

The isolation and identification of exosomes were conducted following our previous procedure (*43*). Briefly, the supernatant of the hiPSC-CMs was collected after cultured in exosome-free medium for 48 hours and centrifuged at 300*g* for 10 min. The cells, membranes, and debris were removed by a series of ultracentrifugation. After filtered through a 0.22 μm filter (Millipore), the supernatant was then ultracentrifuged at 120,000*g* for 90 min to obtain exosomes. Subsequently, the exosomes were resuspended in DPBS and purified at 120,000*g* for 90 min. Last, the exosomes were washed with DPBS and stored at −80°C until use. The protein makers of exosomes (CD9, CD81, Alix, and Syntenin) were examined by Western blotting. The microstructure of exosomes was observed under TEM (Hitachi). The diameter of particles in exosomes was measured using NTA (Zetaview). The zeta potentials of exosomes were analyzed by using a Zetasizer Nano analyzer (Malvern). To visualize the location of exosomes in cells after the uptake by primary cardiomyocytes, PKH-26 was used to label exosomes according to the manufacturer′s instructions (Sigma-Aldrich).

The isolation of primary cardiomyocytes

Neonatal primary cardiomyocytes were isolated from the hearts of 3-day-old Sprague-Dawley rats according to our previous study (*44*). Briefly, hearts were cut into pieces and suspended in 0.08% collagenase type II (GIBCO). Digestion was carried out in a water bath at 4°C for 10 times. After digestion, the supernatant was collected and centrifuged at 200*g* for 5 min. Cells were resuspended in culture medium [Dulbecco′s modified Eagle′s medium (DMEM) + 10% FBS] and plated in a petri dish. To eliminate the contamination of cardiac fibroblasts, cells were preplaced for 2 hours.

In vitro hiPSC-CMs-EXO against oxidative stress in primary cardiomyocytes

The primary cardiomyocytes ($1 \times 10^6/cm^2$) were pretreated with hiPSC-CMs-EXO (80 μg/ml) for 24 hours to ensure that the exosomes could be uptake by the primary cardiomyocytes and then stimulated with H_2O_2 (100 μM) for 4 hours to induce oxidative stress. For JC-1 staining, the MMP in primary cardiomyocytes of each group was detected using the JC-1 kit according to the manufacturer′s instructions (Beyotime). JC-1 (5 mM) was added and incubated for 45 min and then observed under a fluorescence microscope (Olympus). The ratio of red to green fluorescence intensity was analyzed using ImageJ software. For ROS analysis, the intracellular stress levels in primary cardiomyocytes of each group were detected using the Reactive Oxygen Species Assay Kit according to the manufacturer′s instructions (Beyotime). 2′,7′-Dichlorodihydrofluorescein diacetate (DCFH-DA) solution (10 μM) was added and incubated for 20 min and then observed under a fluorescence microscope (Olympus). For MitoTracker staining, the mitochondria morphology in primary cardiomyocytes of each group was detected using the MitoTracker Green Kit according to the manufacturer′s instructions (Beyotime). DCFH-DA solution (20 nM) was added and incubated for 30 min and then observed under a fluorescence microscope (Olympus). For Western blotting analysis, the protein of primary cardiomyocytes in each group were quantified using the BCA protein assay kit (Thermo Fisher Scientific) and examined using Western blotting for the representative proteins of Nrf2 signal pathway (Nrf2, HO-1, and NQO1). The grayscale of protein bands was quantified using the ImageJ software.

Synthesis and characterization of the HAD polymer

The synthesis of the HAD polymer was performed by following our previous work (*12*). In our previous studies, a list of HAD hydrogels with different mass ratios of AEMA and DA was prepared, and the characterization results showed that the adhesive strength of the H-3A-3D (AEMA:DA mass ratio was 3:3) hydrogel showed several times higher than those of the other HAD groups. Therefore, in this study, we also chose the H-3A-3D HAD samples, which showed promising adhesive properties, to prepare the injectable barriers to adhere on the heart surface with continuous movement. Briefly, the HA (1 g) was dissolved in double-distilled H_2O at the concentration of 1% (w/v). Subsequently, EDC (4 mmol), NHS (4 mmol), and AEMA (3 mmol) were added to the HA solutions. Dopamine hydrochloride (DA; 3 mmol) was then added to the solution and stirred for 24 hours. After the reaction, the monomers were dialyzed under acidic conditions for 3 days. The HAD polymers after dialysis were lyophilized and then stored away from light and moisture. HAMA was synthesized by the grafted AEMA group on HA polymer, served as the Ctrl group without the DA group. The chemical structures of HAD and HAMA were determined by ^1H NMR. The shear thinning properties of HAD and HAMA precursors were measured using a rotational rheometer (HAAHE MARS 40, Thermo Fisher Scientific) with the shear rate varying from 0.1 to 1000 s^{-1}. The samples were run in triplicate. The chemical structures of HAD and HAMA were determined by FTIR–attenuated total reflectance (ATR) spectroscopy. FTIR-ATR spectra were recorded in the range of 1300 to 3500 cm^{-1}, acquired by a Nicolet 6700 (Thermo Fisher Scientific) and ZnSE Golden Gate ATR accessory (Specac). Three hundred scans at a resolution of 2 cm^{-1} were averaged for each spectrum. The FTIR spectra were background-subtracted and baseline-corrected with OMNIC software v.8.3.103.

Preparation and characterization of HAD and HAD-EXO hydrogels

For the gelation of HAD, 3 wt % of HAD precursor solution containing LAP (0.1 wt %) (L0290, TCI EUROPE N.V., Zwijndrecht, Belgium) (as the photoinitiator) was prepared. The HAD hydrogels were cross-linked after photocrosslinking under 365 nm of UV

irradiation (7 mW/cm^2) for 10 s. The microstructure of HAD were observed under a SEM (Hitachi). The hiPSC-CMs-EXO was mixed within HAD precursor solution and cross-linked to obtain the HAD-EXO hydrogel. To visualize the distribution of hiPSC-CMs-EXO, the hiPSC-CMs-EXO was prestained with PKH26 (red) according to the manufacturer's instruction (Sigma-Aldrich), and HAD precursor solution was loaded with FITC (green) (50 μg/ml). After photocrosslinking, the HAD+EXOs hydrogel was observed under a laser scanning confocal microscope (NIKON) and then analyzed using ImageJ to distinguish the distribution of red and green fluorescence. For mechanical test, 3 wt % of precursor solution of HAD or HAD+EXOs with 0.1 wt % of LAP was added into cylindrical molds (1 mm thickness and 20 mm diameter). The hydrogels were formed after photocrosslinking under 365 nm of UV irradiation for 10 s. A rheometer (HAAHE MARS 40, Thermo Fisher Scientific) with 20 mm stainless steel parallel plates was used. The parallel plate gap is set to 1 mm. Then, a frequency sweep test was performed at a strain of 1% and frequency from 0.1 to 10 Hz to evaluate the storage modulus (G') and loss modulus (G'') of the hydrogels. For the swelling and degradation test of the hydrogel, 3 wt % of precursory solution with 0.1 wt % of LAP was added into cylindrical molds (4 mm high and 10 mm diameter) to prepare photocrosslinked cylindrical-shaped hydrogel samples. The hydrogels' swelling ratio behavior was assessed by measuring the wet weights of the hydrogels after incubating them in PBS (pH 7.4) at 37°C. Hydrogel samples were taken out at preset time intervals. Immediately after the removal of superficial water using filter papers, the weight of hydrogels was recorded. The swelling ratio (SR) was calculated by the following equation: SR (%) = $(W_t - W_0)/W_0 \times 100\%$, where W_0 and W_t represented the initial weight of the wet hydrogels and the weight after swelling preset time, respectively. The test was repeated three times. For testing the in vitro degradation of the hydrogel, the remaining weight ratio of the hydrogels was assessed by measuring dry weights of the hydrogels (4 mm high and 10 mm diameter) after incubating in PBS (pH 7.4) at 37°C for 4 weeks, with shaking at 100 rpm. At each predetermined time point, the samples were freeze-dried and then weighed. The remaining weight was calculated by the following equation: D_R (%) = $W_r/W_o \times 100\%$, where W_o and W_r represented the initial weight of the freeze-dried hydrogels and the remaining weight of freeze-dried hydrogels after degradation, respectively.

Lap shear test of HAD hydrogels

The lap shear adhesion tests were used to evaluate the adhesive properties of HAD and HAD-EXOs hydrogels before or after photocrosslinking, following our previous study (*4*). Before the lap shear tests, the fresh porcine heart (n = 3 per group) was washed with PBS solution three times. Subsequently, the endocardium and part of the myocardium were removed, leaving the porcine heart wall of 6 mm thickness. Then, the treated porcine heart was cut into 15 mm by 30 mm for the test. Test preparation for the sol-adhesive process is as follows: First, 80 μl of the HAMA or HAD precursor with 0.1 wt % of LAP was smeared evenly on a piece of the treated heart substrate, and the other piece was covered on the hydrogel precursor. The contact area was kept at 10 mm by 10 mm. After that, the adhesive area was cross-linked under 365 nm of UV irradiation for 1 min. Test preparation for the gel-nonadhesive process is as follows: First, 80 μl of the HAMA or HAD precursor with 0.1 wt % of LAP was smeared evenly on the heart substrate. The precursor was then cross-linked under 365 nm of UV irradiation for 1 min. The contact area was kept at 10 mm by 10 mm. After the hydrogel was formed, the inward side of the gel was adherent to the heart, while the outward side of the gel was nonadherent. Subsequently, another heart piece was put onto the outward side surface of the hydrogel. Lap shear tests were performed using the Materials Test System (MTS Criterion 43, MTS Criterion) equipped with a 50 N load cell at a rate of 2.5 mm/min to evaluate the samples' adhesion properties. All these tests were used three times.

In vitro cytocompatibility evaluation of HAD hydrogels

To evaluate the cytocompatibility of HAD hydrogels in vitro, the HAD precursor (3 wt %) was first dissolved in DPBS containing LAP (0.1 wt %) as photoinitiator at room temperature for 3 hours to obtain a homogeneous solution. Fifty microliters of HAD hydrogel [3 wt % (w/v)] was photocrosslinked under UV irradiation at 7 mW/cm^2 for 10 s and store at 4°C until use. Primary CMs isolated from 1- to 2-day neonatal Sprague-Dawley rats were seeded in a 24-well plate at 1×10^5 cells per well and incubated in DMEM containing 10% FBS under standard culture conditions (37°C, 5% CO_2) for 24 hours. After incubation for 24 hours, photocrosslinked HAD hydrogels were moved into the wells and float in the culture medium. The Ctrl group was treated with the culture medium alone. Cellular viability was investigated after cell cultivation with HAD hydrogel. A calcein/PI cell viability/cytotoxicity assay kit (Beyotime, China) was used to assess the biocompatibility of HAD hydrogel. The green color resulted from staining with calcein AM, indicating living cells, and the red color resulted from staining with PI, indicating dead cells. The fluorescence images were taken using a fluorescence microscope (NIKON ECLIPSE Ni). ImageJ software was used to analyze the number of live cells from three randomly selected areas of each sample.

Antiadhesion capacity of HAD in vitro

The antiadhesion capacity of HAD in vitro were performed using L929 fibroblast and RAW264.7 macrophages, which are two cell types commonly found in adhesions in vivo. Briefly, L929 fibroblast (3×10^5/cm^2) or RAW264.7 macrophages (5×10^5/cm^2) were seeded on the surface of HAD hydrogel (n = 4 per group) or glass slides (n = 4 per group) for 24 hours to allow adhere. Cell viability was analyzed using the calcein/PI cell viability/cytotoxicity assay kit (Beyotime, China). After washing the cells with PBS, a PBS solution containing calcein AM (1 μl ml^{-1}, 1 μM) and PI (1 μl ml^{-1}, 0.5 μM) was used to stain the cells for 45 min in the dark and then observed under a fluorescence microscope (NIKON ECLIPSE Ni) and analyzed using the National Institutes of Health ImageJ software. The results of green color indicate the living cells, while the red color indicates the dead cells. Cell viability was expressed as the proportion of viable cells (green) to the total number of cells.

The proliferation properties of L929 cells and RAW264.7 cells on HAD were investigated using the alamarBlue assay kit (Invitrogen, USA). Briefly, L929 fibroblast (2×10^5/cm^2) or RAW264.7 macrophages (3×10^5/cm^2) were seeded on HAD and glass slides. Each group was consisted of four samples, and every sample was added with 1 ml of cell suspension. After culturing for 1 and 3 days, the culture medium was changed with a medium containing 10% (v/v) alamarBlue reagent, and the cells were then incubated at 37°C in 5% CO_2 for 4 hours. Later, 100 μl of solution from each sample was

removed into a 96-well plate. The result was read at 560/590 nm in a BioTek Synergy H1 microplate reader.

Controlled released of hiPSC-CMs-EXO from hydrogels

The hiPSC-CMs-EXO was mixed within a HAD precursor solution at the volume ratio of 1:4 and cross-linked to obtain HAD+EXO hydrogel [final concentration: 3% HAD and hiPSC-CMs-EXO (0.1 μg/μl)]. The exosome release profile in vitro was tested using a micro-BCA protein assay kit (Thermo Fisher Scientific, China). Briefly, the above prepared 100 μl of HAD+EXO hydrogel containing 10 μg of hiPSC-CMs-EXO was photocrosslinking for 20 s using a 365 nm UV light and then placed on the 24-well plates (n = 5), while 200 μl of PBS (pH = 7.4) was added in the wells. With each time point, 100 μl of supernatant was collected and replaced by 100 μl of fresh PBS at days 1, 3, 5, 7, 9, 11, 13, and 15 with five repetition groups. The content of released exosomes was tested, and the percentage of the exosome released was calculated.

Rat pericardial adhesion model

The animal experiments were performed in accordance with the guidelines of the experimental animal administration committee of Southern Medical University (approval number: LAEC-2021-076). Briefly, Sprague-Dawley rats (male; n = 40; 300 ± 20 g) were anesthetized of 2% pentobarbital sodium at a dose of 0.3 ml/100 g by intraperitoneal injection. After removing the partial pericardium, the epicardium was stabbed 100 times with a syringe needle (30 G), and the pericardial cavity was exposed to autologous blood to induce pericardial adhesion. Subsequently, the wound continued to be exposed to the air for 30 min. After that, the model rats were randomly divided into four groups: model (with no further treatment) (n = 10), iCM-EXOs (injected into epicardium directly) (n = 10), HAD (n = 10), and HAD+EXOs (n = 10). For the latter two groups, 100 μl of either HAD or HAD-EXOs precursor solution was carefully pipetted onto the stabbed area, followed by immediate cross-linking using 365 nm of UV light. After surgery, the rats were permitted free access to water and food to recover from the surgery. Throughout the experiments, no obvious infectious complications or dyskinesia was observed. After a duration of 2 or 4 weeks, the rats were euthanized using an overdose of pentobarbital sodium, and the thoracic cavity was exposed to evaluate the postoperative pericardial adhesion. Subsequently, the hearts were harvested, embedded in paraffin wax, and cut into 5 μm slices using a microtome. Heart paraffin sections were stained for H&E to assess the degrees of inflammation.

The retention study in vivo

A subset of rats was administered with ICG (1 mg/ml)–loaded HAD or HAD-EXOs immediately during the induction of pericardial adhesion. Rats were imaged on day 3, day 7, and day 14 after the surgery using the fluorescence imaging system (Digital Precision Medicine Company, Beijing, China) to collect fluorescence intensity.

Gross observation and adhesion score

After 3, 7, 14, and 28 days of surgery, the rats were euthanized with an overdose of sodium pentobarbital and exposed the thoracic cavity to evaluate the postoperative pericardial adhesion. The average adhesion scores and intensities as well as the maximum adhesion intensities were determined using a previously reported method (*9*). The heart was divided into nine segments, and each segment was evaluated an overall adhesion score based on the severity of adhesions from 0 to 4. The degree of adhesion was evaluated following the standard scoring system: score 0, no adhesion; score 1, one thin-film clear adhesion; score 2, moderate and opaque adhesion; score 3, thick adhesion with no vascularization; and score 4, very thick vascularized adhesion or more than one plantar adhesion, requiring sharp dissection. The average adhesion score was reported over these nine segments. The average adhesion intensity was evaluated over all regions that showed adhesion formation. The maximum adhesion intensity score was also evaluated for each animal. At least six rats in each group were evaluated by double-blind scoring.

Histology

The rats were euthanized at a determined time after surgery, and hearts with surrounding adhesive tissues were harvested. To evaluate the fibrous tissues, the hearts were fixed with 4% paraformaldehyde for 24 hours and then embedded in paraffin and sliced into 8 μm thick sections along the short axis transversely across the fibrous zone. To evaluate the antioxidative stress, the hearts were frozen, sectioned into 20 μm thick sections. The heart sections for H&E staining were used to evaluate the parameters of adhesion. The adhesion area was evaluated by ImageJ software. For immunofluorescence staining, the heart sections were incubated with anti–MSR-1 rabbit monoclonal antibody (1:300; Bioss, China) or anti–Gata binding factor 6 (GATA6) rabbit monoclonal antibody (1:300; Affnity) and subjected to incubation with goat anti-rabbit Alexa Fluor Cy3-conjugated secondary antibody (1:500; Abcam). Last, the nucleus was stained with 4′,6-diamidino-2-phenylindole solution (Beyotime) and then observed under a fluorescence microscope (Olympus).

Reverse transcription qPCR

Total RNA was isolated using TRIzol reagent (Invitrogen, China) following the manufacturer′s instructions. One milligram of RNA was used to synthesize cDNA using a reverse transcription reagent kit (Takara, China). The reverse transcription qPCR (qRT-PCR) was carried out according to the protocol and conducted with an Applied Biosystems 7500 fast real-time PCR system with the following temperature profile: 95°C for 30 s, denaturation at 95°C for 5 s, and annealing/extension at 60°C for 30 s for 40 cycles. Primers sequences used for qRT-PCR were shown in table S1. The relative expression of the genes was calculated using the $2^{-\Delta\Delta Cq}$ method, and the gene expression was normalized to the housekeeping gene GAPDH (glyceraldehyde-3-phosphate dehydrogenase) in the same sample.

ELISA detection

After 7 days of surgery, the rats were euthanized with an overdose of sodium pentobarbital, and the arterial blood was extracted with a syringe exposed to evaluate the serum inflammation level. The concentrations of IL-1β, IL-6, and TNF-α in the serum were analyzed by ELISA according to the manufacturer′s instruction (Moshake Biotechnology, China).

Detection of tissue SOD and GSH

After 7 days of surgery, the rats were euthanized with an overdose of sodium pentobarbital and the hearts were harvested. First, the heart

samples were prepared by adding 100 μl of SOD sample preparation or 100 μl of protein removal reagent M solution per 10 mg of tissue block, homogenized using a freezing homogenizer (Thermo Fisher Scientific, USA), and the supernatant was obtained by centrifugation at 12,000*g* for 5 to 10 min. The supernatant was reacted by adding the assay solution according to the manufacturer's procedure of the SOD assay kit (Beyotime, China) or GSH assay kit (Beyotime, China). The absorbance values were detected under an enzyme standardizer (Thermo Fisher Scientific, USA), and the tissue SOD and GSH contents were calculated according to the respective standard curves.

Cardiac function analysis

After 4 weeks after surgery, the rats were anesthetized, and echocardiographic examination was conducted by Vevo 2100 echocardiography (Vevo2100, VisualSonics, USA) equipped with a MS400 transducer (18 to 38 MHz). Cardiac function parameters including LVIDd, LVIDs, left ventricular ejection fraction, and left ventricular fractional shortening were measured.

Statistical analysis

Experiments were run in at least triplicate for each sample ($n \geq 3$). The experimental data were analyzed via using one-way analysis followed by Tukey's significant difference post hoc test. The results were obtained from at least six images of three independent replications of the samples.

Supplementary Materials

This PDF file includes:
Figs. S1 to S13
Table S1
Legends for movies S1 to S4

Other Supplementary Material for this manuscript includes the following:
Movies S1 to S4

REFERENCES AND NOTES

1. V. Bianco, A. Kilic, T. G. Gleason, E. Aranda-Michel, A. Habertheuer, Y. Wang, F. Navid, A. Kacin, I. Sultan, Reoperative cardiac surgery is a risk factor for long-term mortality. *Ann. Thorac. Surg.* **110**, 1235–1242 (2020).
2. C. B. Park, R. M. Suri, H. M. Burkhart, K. L. Greason, J. A. Dearani, H. V. Schaff, T. M. Sundt III, Identifying patients at particular risk of injury during repeat sternotomy: Analysis of 2555 cardiac reoperations. *J. Thorac. Cardiovasc. Surg.* **140**, 1028–1035 (2010).
3. J. P. Jacobs, C. Mavroudis, J. A. Quintessenza, P. J. Chai, S. K. Pasquali, K. D. Hill, L. A. Vricella, M. L. Jacobs, J. A. Dearani, D. Cameron, Reoperations for pediatric and congenital heart disease: An analysis of the Society of Thoracic Surgeons (STS) congenital heart surgery database. *Semin. Thorac. Cardiovasc. Surg. Pediatr. Card. Surg. Annu.* **17**, 2–8 (2014).
4. A. Cannata, D. Petrella, C. F. Russo, G. Bruschi, P. Fratto, M. Gambacorta, L. Martinelli, Postsurgical intrapericardial adhesions: Mechanisms of formation and prevention. *Ann. Thorac. Surg.* **95**, 1818–1826 (2013).
5. U. U. Nkere, S. A. Whawell, C. E. Sarraf, J. B. Schofield, J. N. Thompson, K. M. Taylor, Pericardial trauma and adhesions in relation to reoperative cardiac surgery. *Thorac. Cardiov. Surg.* **43**, 338–346 (1995).
6. F. J. Giordano, Oxygen, oxidative stress, hypoxia, and heart failure. *J. Clin. Invest.* **115**, 500–508 (2005).
7. H. Tsutsui, S. Kinugawa, S. Matsushima, Oxidative stress and heart failure. *Am. J. Physiol. Heart Circ. Physiol.* **301**, H2181–H2190 (2011).
8. J. Iliopoulos, G. B. Cornwall, R. O. N. Evans, C. Manganas, K. A. Thomas, D. C. Newman, W. R. Walsh, Evaluation of a bioabsorable polylactide film in a large animal model for the reduction of retrosternal adhesions. *J. Surg. Res.* **118**, 144–153 (2004).
9. M. Fujita, G. M. Policastro, A. Burdick, H. T. Lam, J. L. Ungerleider, R. L. Braden, D. Huang, K. G. Osborn, J. H. Omens, M. M. Madani, K. L. Christman, Preventing post-surgical cardiac adhesions with a catechol-functionalized oxime hydrogel. *Nat. Commun.* **12**, 3764 (2021).
10. L. M. Stapleton, A. N. Steele, H. Wang, H. Lopez Hernandez, A. C. Yu, M. J. Paulsen, A. A. A. Smith, G. A. Roth, A. D. Thakore, H. J. Lucian, K. P. Totherow, S. W. Baker, Y. Tada, J. M. Farry, A. Eskandari, C. E. Hironaka, K. J. Jaatinen, K. M. Williams, H. Bergamasco, C. Marschel, B. Chadwick, F. Grady, M. Ma, E. A. Appel, Y. J. Woo, Use of a supramolecular polymeric hydrogel as an effective post-operative pericardial adhesion barrier. *Nat. Biomed. Eng.* **3**, 611–620 (2019).
11. W. Liang, W. He, R. Huang, Y. Tang, S. Li, B. Zheng, Y. Lin, Y. Lu, H. Wang, D. Wu, Peritoneum-inspired Janus porous hydrogel with anti-deformation, anti-adhesion, and pro-healing characteristics for abdominal wall defect treatment. *Adv. Mater.* **34**, 2108992 (2022).
12. X. Wu, W. Guo, L. Wang, Y. Xu, Z. Wang, Y. Yang, L. Yu, J. Huang, Y. Li, H. Zhang, Y. Wu, G. Li, W. Huang, An injectable asymmetric-adhesive hydrogel as a $GATA^{6+}$ cavity macrophage trap to prevent the formation of postoperative adhesions after minimally invasive surgery. *Adv. Funct. Mater.* **32**, 2110066 (2022).
13. C. Cui, T. Wu, X. Chen, Y. Liu, Y. Li, Z. Xu, C. Fan, W. Liu, A Janus hydrogel wet adhesive for internal tissue repair and anti-postoperative adhesion. *Adv. Funct. Mater.* **30**, 2005689 (2020).
14. L. Gao, L. Wang, Y. Wei, P. Krishnamurthy, G. P. Walcott, P. Menasché, J. Zhang, Exosomes secreted by hiPSC-derived cardiac cells improve recovery from myocardial infarction in swine. *Sci. Transl. Med.* **12**, eaay1318 (2020).
15. S. B. Andugulapati, K. Gourishetti, S. K. Tirunavalli, T. B. Shaikh, R. Sistla, Biochanin-A ameliorates pulmonary fibrosis by suppressing the TGF-β mediated EMT, myofibroblasts differentiation and collagen deposition in in vitro and in vivo systems. *Phytomedicine* **78**, 153298 (2020).
16. L. Chen, Y. Wang, Y. Pan, L. Zhang, C. Shen, G. Qin, M. Ashraf, N. Weintraub, G. Ma, Y. Tang, Cardiac progenitor-derived exosomes protect ischemic myocardium from acute ischemia/reperfusion injury. *Biochem. Biophys. Res. Commun.* **431**, 566–571 (2013).
17. Y. Wang, L. Zhang, Y. Li, L. Chen, X. Wang, W. Guo, X. Zhang, G. Qin, S.-h. He, A. Zimmerman, Y. Liu, I.-m. Kim, N. L. Weintraub, Y. Tang, Exosomes/microvesicles from induced pluripotent stem cells deliver cardioprotective miRNAs and prevent cardiomyocyte apoptosis in the ischemic myocardium. *Int. J. Cardiol.* **192**, 61–69 (2015).
18. M. R. Santoso, G. Ikeda, Y. Tada, J. H. Jung, E. Vaskova, R. G. Sierra, C. Gati, A. B. Goldstone, D. von Bornstaedt, P. Shukla, Exosomes from induced pluripotent stem cell–derived cardiomyocytes promote autophagy for myocardial repair. *J. Am. Heart Assoc.* **9**, e014345 (2020).
19. B. Liu, B. W. Lee, K. Nakanishi, A. Villasante, R. Williamson, J. Metz, J. Kim, M. Kanai, L. Bi, K. Brown, G. Di Paolo, S. Homma, P. A. Sims, V. K. Topkara, G. Vunjak-Novakovic, Cardiac recovery via extended cell-free delivery of extracellular vesicles secreted by cardiomyocytes derived from induced pluripotent stem cells. *Nat. Biomed. Eng.* **2**, 293–303 (2018).
20. F. J. Verweij, C. Revenu, G. Arras, F. Dingli, D. Loew, D. M. Pegtel, G. Follain, G. Allio, J. G. Goetz, P. Zimmermann, P. Herbomel, F. Del Bene, G. Raposo, G. van Niel, Live tracking of inter-organ communication by endogenous exosomes in vivo. *Dev. Cell* **48**, 573–589.e4 (2019).
21. Z. Wan, L. Zhao, F. Lu, X. Gao, Y. Dong, Y. Zhao, M. Wei, G. Yang, C. Xing, L. Liu, Mononuclear phagocyte system blockade improves therapeutic exosome delivery to the myocardium. *Theranostics* **10**, 218–230 (2020).
22. P. Chen, L. Wang, X. Fan, X. Ning, B. Yu, C. Ou, M. Chen, Targeted delivery of extracellular vesicles in heart injury. *Theranostics* **11**, 2263–2277 (2021).
23. C. W. Chen, L. L. Wang, S. Zaman, J. Gordon, M. F. Arisi, C. M. Venkataraman, J. J. Chung, G. Hung, A. C. Gaffey, L. A. Spruce, H. Fazelinia, R. C. Gorman, S. H. Seeholzer, J. A. Burdick, P. Atluri, Sustained release of endothelial progenitor cell-derived extracellular vesicles from shear-thinning hydrogels improves angiogenesis and promotes function after myocardial infarction. *Cardiovasc. Res.* **114**, 1029–1040 (2018).
24. C. Han, J. Zhou, C. Liang, B. Liu, X. Pan, Y. Zhang, Y. Wang, B. Yan, W. Xie, F. Liu, X.-Y. Yu, Y. Li, Human umbilical cord mesenchymal stem cell derived exosomes encapsulated in functional peptide hydrogels promote cardiac repair. *Biomater. Sci.* **7**, 2920–2933 (2019).
25. J. A. Burdick, G. D. Prestwich, Hyaluronic acid hydrogels for biomedical applications. *Adv. Mater.* **23**, H41–H56 (2011).
26. E. Lih, J. S. Lee, K. M. Park, K. D. Park, Rapidly curable chitosan–PEG hydrogels as tissue adhesives for hemostasis and wound healing. *Acta Biomater.* **8**, 3261–3269 (2012).
27. J. Zindel, M. Peiseler, M. Hossain, C. Deppermann, W. Y. Lee, B. Haenni, B. Zuber, J. F. Deniset, B. G. J. Surewaard, D. Candinas, P. Kubes, Primordial GATA6 macrophages function as extravascular platelets in sterile injury. *Science* **371**, eabe0595 (2021).
28. G. M. Saed, W. Zhang, M. P. Diamond, Molecular characterization of fibroblasts isolated from human peritoneum and adhesions. *Fertil. Steril.* **75**, 763–768 (2001).

29. X. Z. Shu, K. Ghosh, Y. Liu, F. S. Palumbo, Y. Luo, R. A. Clark, G. D. Prestwich, Attachment and spreading of fibroblasts on an RGD peptide–modified injectable hyaluronan hydrogel. *J. Biomed. Mater. Res. A* **68A**, 365–375 (2004).
30. H. Li, B. Yu, P. Yang, J. Zhan, X. Fan, P. Chen, X. Liao, C. Ou, Y. Cai, M. Chen, Injectable AuNP-HA matrix with localized stiffness enhances the formation of gap junction in engrafted human induced pluripotent stem cell-derived cardiomyocytes and promotes cardiac repair. *Biomaterials* **279**, 121231 (2021).
31. S.-H. Kim, K. Kim, B. S. Kim, Y.-H. An, U.-J. Lee, S.-H. Lee, S. L. Kim, B.-G. Kim, N. S. Hwang, Fabrication of polyphenol-incorporated anti-inflammatory hydrogel via high-affinity enzymatic crosslinking for wet tissue adhesion. *Biomaterials* **242**, 119905 (2020).
32. Z. Guo, S. Mi, W. Sun, The multifaceted nature of catechol chemistry: Bioinspired pH-initiated hyaluronic acid hydrogels with tunable cohesive and adhesive properties. *J. Mater. Chem. B* **6**, 6234–6244 (2018).
33. W. Zhang, R. Wang, Z. Sun, X. Zhu, Q. Zhao, T. Zhang, A. Cholewinski, F. K. Yang, B. Zhao, R. Pinnaratip, P. K. Forooshani, B. P. Lee, Catechol-functionalized hydrogels: Biomimetic design, adhesion mechanism, and biomedical applications. *Chem. Soc. Rev.* **49**, 433–464 (2020).
34. X. Xu, X. Xia, K. Zhang, A. Rai, Z. Li, P. Zhao, K. Wei, L. Zou, B. Yang, W.-K. Wong, P. W.-Y. Chiu, L. Bian, Bioadhesive hydrogels demonstrating pH-independent and ultrafast gelation promote gastric ulcer healing in pigs. *Sci. Transl. Med.* **12**, eaba8014 (2020).
35. Y. Xiong, L. Chen, C. Yan, W. Zhou, Y. Endo, J. Liu, L. Hu, Y. Hu, B. Mi, G. Liu, Circulating exosomal miR-20b-5p inhibition restores Wnt9b signaling and reverses diabetes-associated impaired wound healing. *Small* **16**, 1904044 (2020).
36. M. Gartz, A. Darlington, M. Z. Afzal, J. L. Strande, Exosomes exert cardioprotection in dystrophin-deficient cardiomyocytes via ERK1/2-p38/MAPK signaling. *Sci. Rep.* **8**, 16519 (2018).
37. X. He, H. Kan, L. Cai, Q. Ma, Nrf2 is critical in defense against high glucose-induced oxidative damage in cardiomyocytes. *J. Mol. Cell. Cardiol.* **46**, 47–58 (2009).
38. X. Liu, X. Yuan, G. Liang, S. Zhang, G. Zhang, Y. Qin, Q. Zhu, Q. Xiao, N. Hou, J.-D. Luo, BRG1 protects the heart from acute myocardial infarction by reducing oxidative damage through the activation of the NRF2/HO1 signaling pathway. *Free Radic. Biol. Med.* **160**, 820–836 (2020).
39. N. Colak, Y. Nazli, M. F. Alpay, O. N. Aksoy, I. O. Akkaya, R. Bayrak, O. Cakir, Effect of topical N-acetylcysteine in the prevention of postoperative pericardial adhesion formation in a rabbit model. *Cardiovasc. Pathol.* **22**, 368–372 (2013).
40. A. M. Alizzi, P. Summers, V. H. Boon, J.-P. Tantiongco, T. Thompson, B. J. Leslie, D. Williams, M. Steele, B. P. Bidstrup, A.-M. A. Diqer, Reduction of post-surgical pericardial adhesions using a pig model. *Heart Lung Circ.* **21**, 22–29 (2012).
41. M. P. Diamond, E. L. Burns, B. Accomando, S. Mian, L. Holmdahl, Seprafilm® adhesion barrier:(1) A review of preclinical, animal, and human investigational studies. *Gynecol. Surg.* **9**, 237–245 (2012).
42. A. Bel, L. Kachatryan, P. Bruneval, S. Peyrard, C. Gagnieu, J.-N. Fabiani, P. Menasché, A new absorbable collagen membrane to reduce adhesions in cardiac surgery. *Interact. Cardiovasc. Thorac. Surg.* **10**, 213–216 (2010).
43. P. Chen, X. Ning, W. Li, Y. Pan, L. Wang, H. Li, X. Fan, J. Zhang, T. Luo, Y. Wu, C. Ou, M. Chen, Fabrication of Tβ4-exosome-releasing artificial stem cells for myocardial infarction therapy by improving coronary collateralization. *Bioact. Mater.* **14**, 416–429 (2022).
44. L. Wang, Y. Wu, T. Hu, B. Guo, P. X. Ma, Electrospun conductive nanofibrous scaffolds for engineering cardiac tissue and 3D bioactuators. *Acta Biomater.* **59**, 68–81 (2017).

Acknowledgments: We thank X. Fan for conducting the animal experiments and X. Chen for assistance with the methodology. **Funding:** This work was funded by the National Key R&D Program of China (no. 2022YFB4600600) and the National Natural Science Foundation of China (nos. 32271423, 32000955, 82172103, and 81871504). **Author contributions:** Conceptualization and supervision: L.W., C.O., W.H., and Y.W. Writing—original draft: L.W. Writing—review and editing: L.W., P.C., and Y.W. Methodology: L.W., P.C., Y.P., Z.W., J.X., X.W., Q.Y., M.L., and S.L. Visualization: Y.P., Z.W., M.L., and S.L. Investigation: L.W., P.C., X.W., and Y.W. **Competing interests:** The authors declare that they have no competing interests. **Data and materials availability:** All data needed to evaluate the conclusions in the paper are present in the paper and/or the Supplementary Materials.

Submitted 15 February 2023
Accepted 6 July 2023
Published 4 August 2023
10.1126/sciadv.adh1753